AD_____

Award Number:
W81XWH-08-1-0716

TITLE:

Development of Lipid-based Nanoparticles for in vivo Targeted Delivery of Imaging Agents into Breast Cancer Cells

PRINCIPAL INVESTIGATOR:
Anatoliy V. Popov, Ph.D.

CONTRACTING ORGANIZATION:
University of Pennsylvania
Philadelphia, PA 19107

REPORT DATE:

April 2010

TYPE OF REPORT:
Final

PREPARED FOR: U.S. Army Medical Research and Materiel Command
Fort Detrick, Maryland 21702-5012

DISTRIBUTION STATEMENT:

X Approved for public release; distribution unlimited

REPORT DOCUMENTATION PAGE

Form Approved
OMB No. 0704-0188

1. REPORT DATE *(DD-MM-YYYY)*	2. REPORT TYPE	3. DATES COVERED *(From - To)*
01-04-2010	Final	15 SEP 2008 - 14 MAR 2010

4. TITLE AND SUBTITLE
Development of Lipid-based Nanoparticles for in vivo Targeted Delivery of Imaging Agents into Breast Cancer Cells

5a. CONTRACT NUMBER

5b. GRANT NUMBER
W81XWH-08-1-0716

5c. PROGRAM ELEMENT NUMBER

6. AUTHOR(S)
Anatoliy V. Popov, Ph.D. (project PI)

Yuri Sykulev, M.D., Ph.D. (subconcontract PI)

5d. PROJECT NUMBER

5e. TASK NUMBER

5f. WORK UNIT NUMBER

7. PERFORMING ORGANIZATION NAME(S) AND ADDRESS(ES)
University of Pennsylvania
Philadelphia, PA 19104
Email:
avpopov@mail.med.upenn.edu

8. PERFORMING ORGANIZATION REPORT NUMBER

9. SPONSORING / MONITORING AGENCY NAME(S) AND ADDRESS(ES)
U.S. Army Medical Research and Materiel Command
Fort Detrick,
Maryland 21702-5012

10. SPONSOR/MONITOR'S ACRONYM(S)

11. SPONSOR/MONITOR'S REPORT NUMBER(S)

12. DISTRIBUTION / AVAILABILITY STATEMENT
Approved for public release; distribution unlimited

13. SUPPLEMENTARY NOTES

14. ABSTRACT Breast cancer represents a unique disease in oncology, in that specific markers have been identified and are routinely used for diagnosis and targeted therapy. Targeted delivery of a combined imaging and therapy agent to cancer cells is an avenue to develop a new generation of effective and selective anticancer agents. The goal of this proposal is to develop novel nanoparticles for *in vivo* breast cancer targeting. The nanoparticles consist of a cholesterol ester core surrounded with a lipid monolayer shell containing an imaging agent and metal chelating groups that can attach proteins of interest through specific His_6 tagging. We have synthesized nanoparticle building blocks as well as imaging agents consisting from the near infrared fluorophore pyropheophorbide a conjugated with core or shell lipids. Varying the core composition we have assembled a series of the nanoparticles with size from 8 nm for smallest one to 20 nm for largest nanoparticle. We have shown that the nanoparticles with cholesterol oleate core have supreme shelf-life and stability at the conditions close to physiological. We have prepared a number of lipid nanoparticles with His_6-tagged targeting proteins, which were successfully tested *in vitro* for specific targeting of model cell lines. We have shown that due to multivalent nature of the targeting nanoparticles the wide spectrum of proteins from natural low affinity receptor ($<10^4$ M^{-1}) to antibody Fab fragment ($>10^7$ M^{-1}) can be used in nanoparticle composition. Time course analysis of the nanoparticle binding to the cell surface revealed that the shell loaded imaging agent is much more effective than the core loaded one.

15. SUBJECT TERMS
Breast Cancer, Nanoparticles, Near Infrared Optical Imaging, Magnetic Resonance Imaging, Targeted Delivery, Porphyrins, Photodynamic Therapy, Epidermal Growth Factor Receptor, HER-2/neu

16. SECURITY CLASSIFICATION OF:			17. LIMITATION OF ABSTRACT	18. NUMBER OF PAGES	19a. NAME OF RESPONSIBLE PERSON
					USAMRMC
a. REPORT	b. ABSTRACT	c. THIS PAGE	UU	5	19b. TELEPHONE NUMBER *(include area code)*
U	U	U		2	

Table of Contents

1. Introduction

Targeted delivery of imaging and therapeutic agents to cancer cells is thought to be effective diagnostic and therapeutic modalities to diagnose and treat breast cancer[1,2]. Application of lipid-based platform for the delivery appears to be one of the most promising approaches due to a low toxicity and biodegradable nature of this platform[3]. Thus far, liposomes have been extensively utilized to develop various delivery systems. There are several problems, however, with the liposome delivery system that needs to be overcome to improve the specificity and effectiveness of the delivery[4].

First, liposomes that are currently available have relatively large size, i.e., 100-200 nm, and can be effectively captured by reticuloendothelial system decreasing the specificity and effectiveness of targeting.

Second, incorporation of ligands into the liposomes that determine the specificity of the targeting often requires chemical modification of these ligands that could result in loss of ligands biological activity.

Third, ligands that are often used for specific targeting of liposomes are not natural ligands of receptors of interest and, therefore, less likely would induce endocytosis; meanwhile, the latter facilitates both specificity and effectiveness of the targeting. In addition, natural ligands are less likely to be immunogenic as opposed to antibodies that could elicit unwanted immune response.

We propose to developed novel lipid-based nanoparticles that have size around 10 nm and possess next features:

(i) hydrophobic core surrounded by lipid based monolayer that results in formation of biodegradable nanoparticles with increased stability;

(ii) conjugation of imaging and therapeutic agents with lipid components of the nanoparticle core that result in stable entrapment of the agents leading to increased specificity of targeted delivery;

(iii) incorporation of Ni-NTA moieties into lipid shell that permits effective immobilization of protein ligands on the nanoparticles surface via C-terminal hexahistidyl-tag and bypasses any chemical modifications of the ligands.

In this grant, we have proposed to demonstrate in proof-of principle the fabrication feasibility of such universal multimodal lipid-based biodegradable platform. We will measure the size, stability and *in vitro* specificity of the nanoparticles. These data will be used for submission a grant to further improvement of the nanoparticles and study the nanoparticle specificity and effectiveness of the delivery of imaging and therapeutic agents *in vivo*.

2. Body

2.1. Research Overview

Targeted delivery of imaging and therapeutic agents to cancer or infected cells is one of the most effective diagnostic and therapeutic modalities to treat human diseases. Rapid development of nanotechnology opens new possibilities to design various nanoplatforms to combine imaging and/or therapeutic agents for targeting delivery. The most widely used nanoplatforms thus far are semiconductor quantum dots, iron oxide and gold nanocrystals, dendrimers or small sized uniform polymer, and various lipid-based nanoparticles [2,5]. A common problem in developing the nanoplatforms is *in vivo* nanoparticle biodegradability, which is related to particles short- and long-term toxicity. The lipid-based nanoparticles are an excellent example of non-toxic and completely biodegradable nanoparticles.

To develop universal multimodal lipid-based nanoparticles that could carry imaging compounds for visualization cancer cells, we have opted to create lipid-based nanoparticles composed of hydrophobic cholesterol esters core[6] and PEGylated shell lipids. While the shell is designed to carry imaging agents, it is primarily made to contain metal-chelating groups that attached targeting molecules to the nanoparticles through interaction with targeting molecule His-tag. The core stabilizes nanoparticles and can also bear imaging agents. Imaging agents are being synthesized as Near Infrared (NIR) dye-lipid conjugates[7]. The nanoparticles are to be conjugated with a natural ligand as well as with a recombinant Fab fragment of antibody and used to investigate their binding to target cell surface and stability in serum containing media. These data will provide information about potential of the nanoparticles as *in vivo* imaging agent.

The research therefore consists of three major parts:

(i) Synthesis of imaging agents (NIR dye-lipid conjugates and Gd-lipid chelates) and nanoparticles building block (core component);

(ii) Nanoparticles assembly and size measurements;

(iii) *In vitro* imaging of model cells with the lipid nanoparticles and studying their stability.

The project is ongoing and the obtained results presented and discussed below.

2.2. Results

2.2.1. Synthesis of imaging agents

Synthesis of pyropheophorbide *a* (Pyro).

Synthesis of Pyropheophorbide *a* (λ_{abs} 660 nm, λ_{em} 725 nm) from *Spirulina Pacifica* algae is presented in Scheme 1.

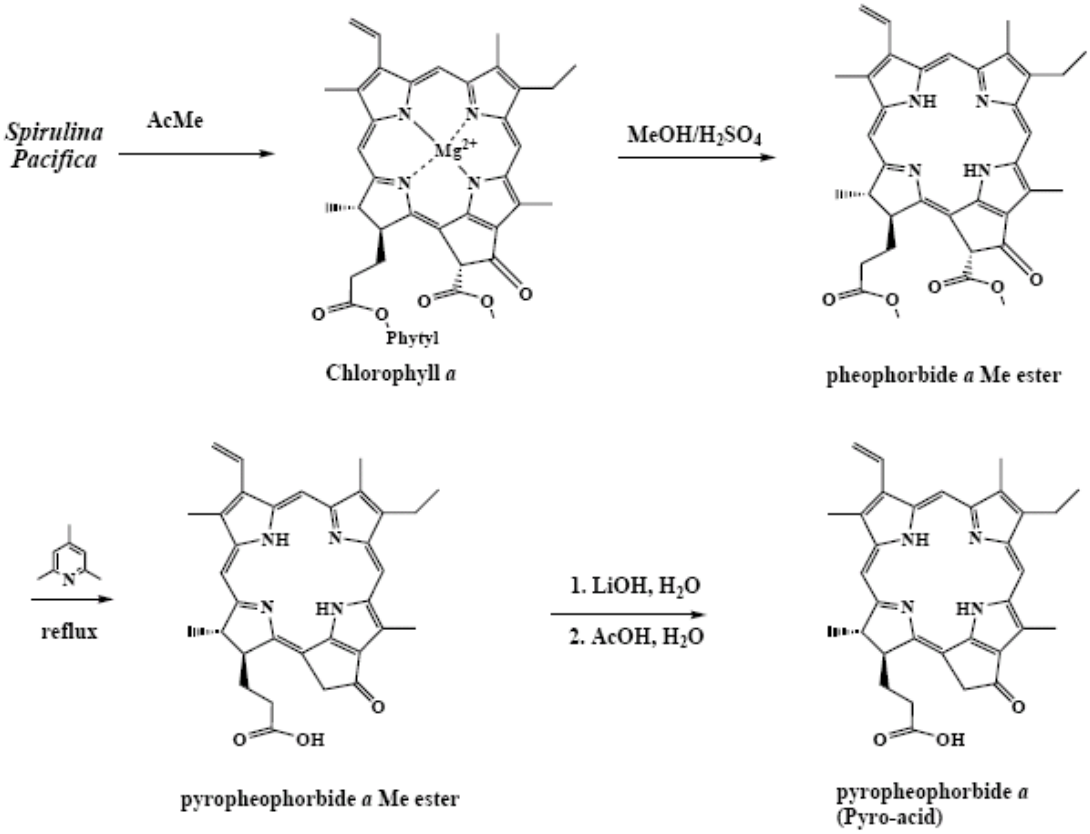

Scheme 1. Synthesis of pyropheophorbide *a*

1.5 g of Pyro-acid was obtained from 1.5 kg of Spirulina Pacifica. Pyro-acid was used in syntheses of imaging components both for the nanoparticle s core (Pyro-CE-OA) and shell Pyro-PE (*vide infra*).

Synthesis of 1-palmytoyl-2-pyropheophorboyl-*sn*-glycero-3-phosphatidyl-ethanol amine (Pyro-PE)

Synthesis of Pyro-PE from N-Boc protected *Lyso*-PE and Pyro acid is depicted in Scheme 2. (This is an original synthesis. The deta ils will be published in article [7], which is s ubmitted to the Journa l of the American Chemical Society. See **Appendices**.)

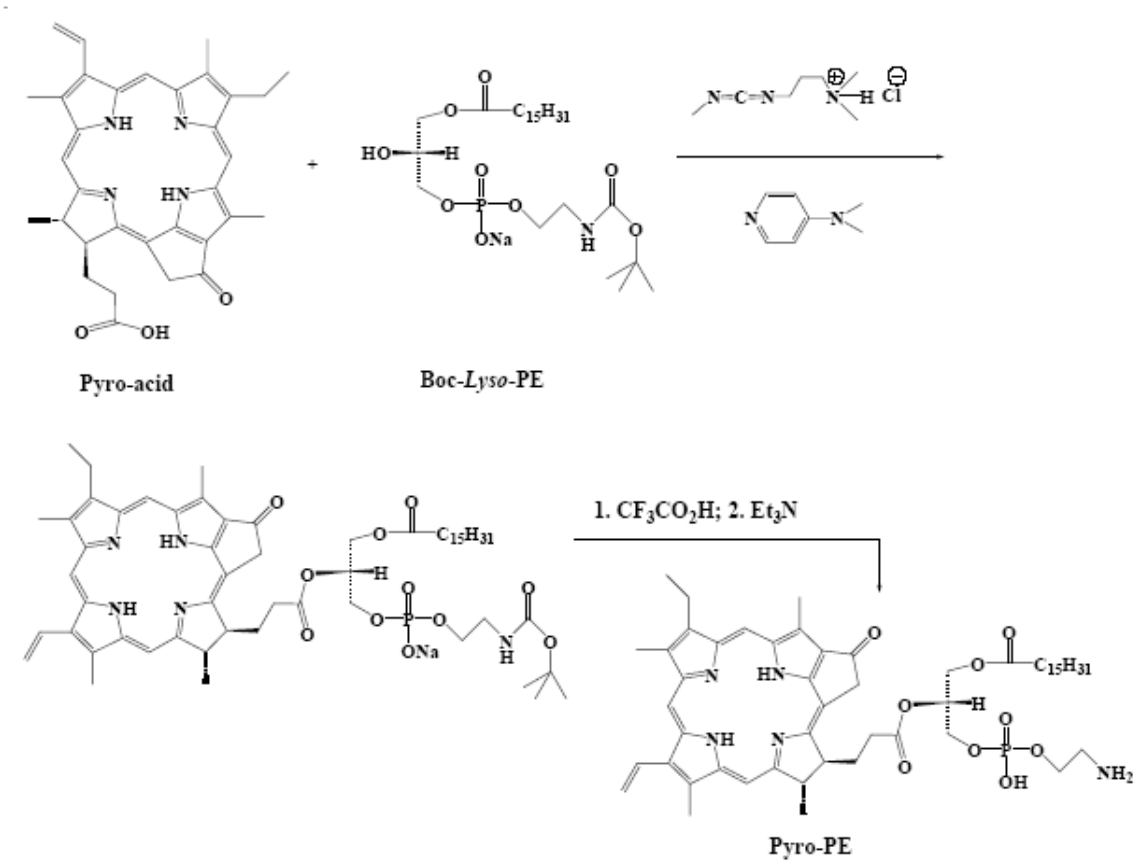

Scheme 2. Synthesis of 1-palmytoyl-2-pyropheophorboyl-*sn*-glycero-3-phosphatidyl-ethano amine (Pyro-PE)

40 mg of Pyro-PE was obtained and used for shell image loading of the lipid nanoparticles.

Synthesis of 5-Androsten-17*β*-pyropheophorboyl-amino-3*β*-yl Oleate (Pyro-CE-OA)

We have developed a completely new two-step synthesis of 5-Androsten-17 *β*-pyropheophorboyl-amino-3*β*-yl Ole ate (Pyro -CE-OA). This s ynthetic pathway is presented in Scheme 3.

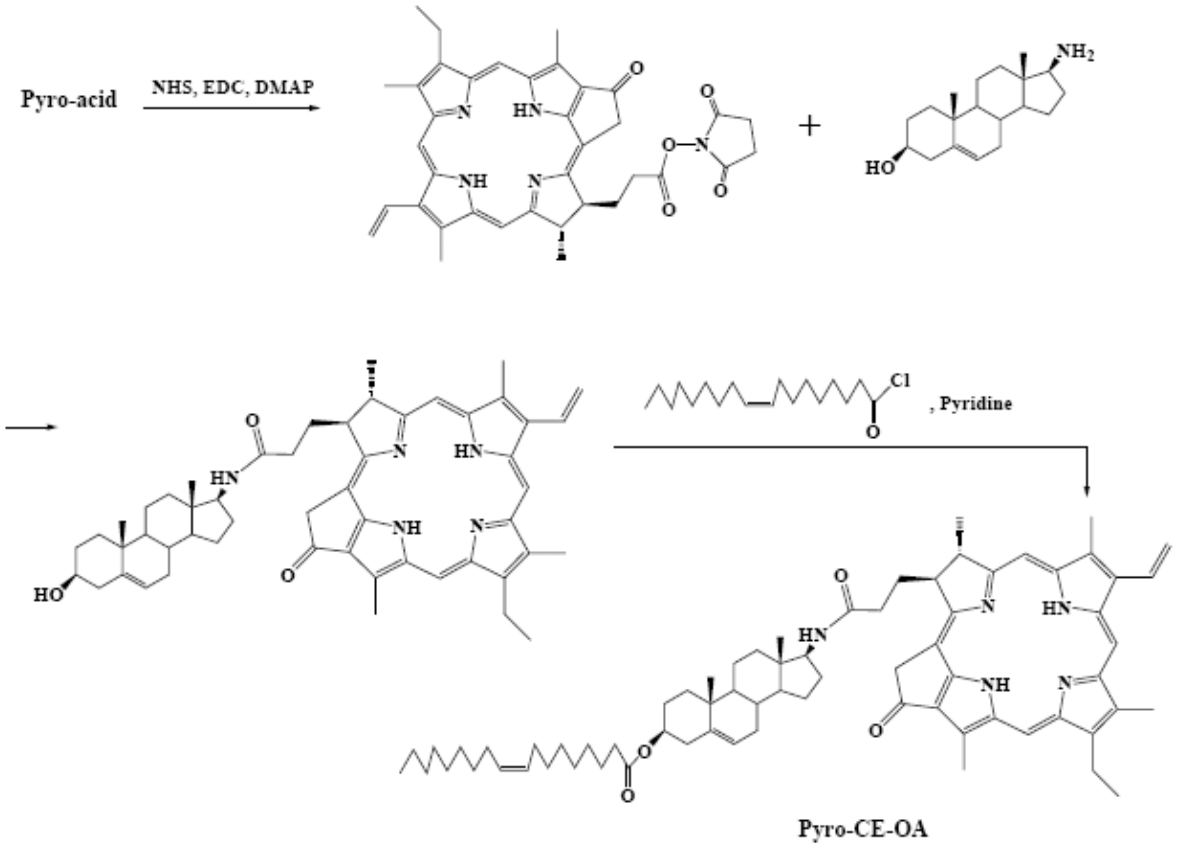

Scheme 3. Synthesis of 5-Androsten-17*β*-pyropheophorboyl-amino-3*β*-yl Oleate (Pyro-CE-OA)

140 mg of Pyro-CE-OA was obtained and used for core image loading of the lipid nanoparticles. ^{1}H NMR ($CDCl_3$): 9.37, 9.33, and 8.55 (each s, 1H, 5-H, 10-H, and 20-H of pyro); 8.00 (dd, J = 17.7, 11.4 Hz, 1H, 3 ^{1}-CH=CH_2 of Pyro); 6.28 (d, J = 17.7 Hz, 1H, *trans*-3^2-CH=CH_2 of pyro); 6.17 (d, J = 11.4 Hz, 1H, *cis*-3^2-CH=CH_2 of pyro); 5.31 (m , 3H, 2 x vinyl-H and 6-H of oleate), 5.23 (ABX, 2H, 13^2-CH_2 of pyro); 5.02 (m , 1H, N-H of cholesterol), 4.55 (m, 2H, 18-H of pyro, 3-H of cholesterol); 4.35 (m , J = 7.8 Hz, 1H for 17-H of pyro); 3.75 (m , 1H, 17-H of cholesterol), 3.63 (q, J = 7.4 Hz, 2H, 8-C H_2CH$_3$ of Pyro); 3.47, 3.46 and 3.23 (each s, 3H, 12-CH3, 2-CH$_3$ and 7-CH$_3$ of pyro); 2. 71 and 2.46 (each m , 2H, for 2 x 17 ^{1}-H and 2 x 17 ^{2}-H of pyro); 2.22 (m, 6H of cholesterol oleate), 2.10-1.75 (m, 11H of cholesterol oleate), 1.70-0.95 (m, 39H of cholesterol oleate), 1.82 (d, J = 7.2 Hz, 3H, 18-CH$_3$ of Pyro); 1.65 (t, J = 8.3 Hz, 3H, 8-CH_2CH_3 of pyro), 0.88 (m , 6H, 19- CH$_3$ of cholesterol and term inal CH$_3$ of oleate), 0.32 (s, 3H, 18-CH$_3$ of cholesterol).

Synthesis of diethylenetriamine pentaacetic acid bis-stearylamide Gagolinium salt monohydrate (DTPA-DSA-Gd)

Synthesis of diethylenetriamine pentaacetic acid bis-stearylamide (DTPA-DSA).

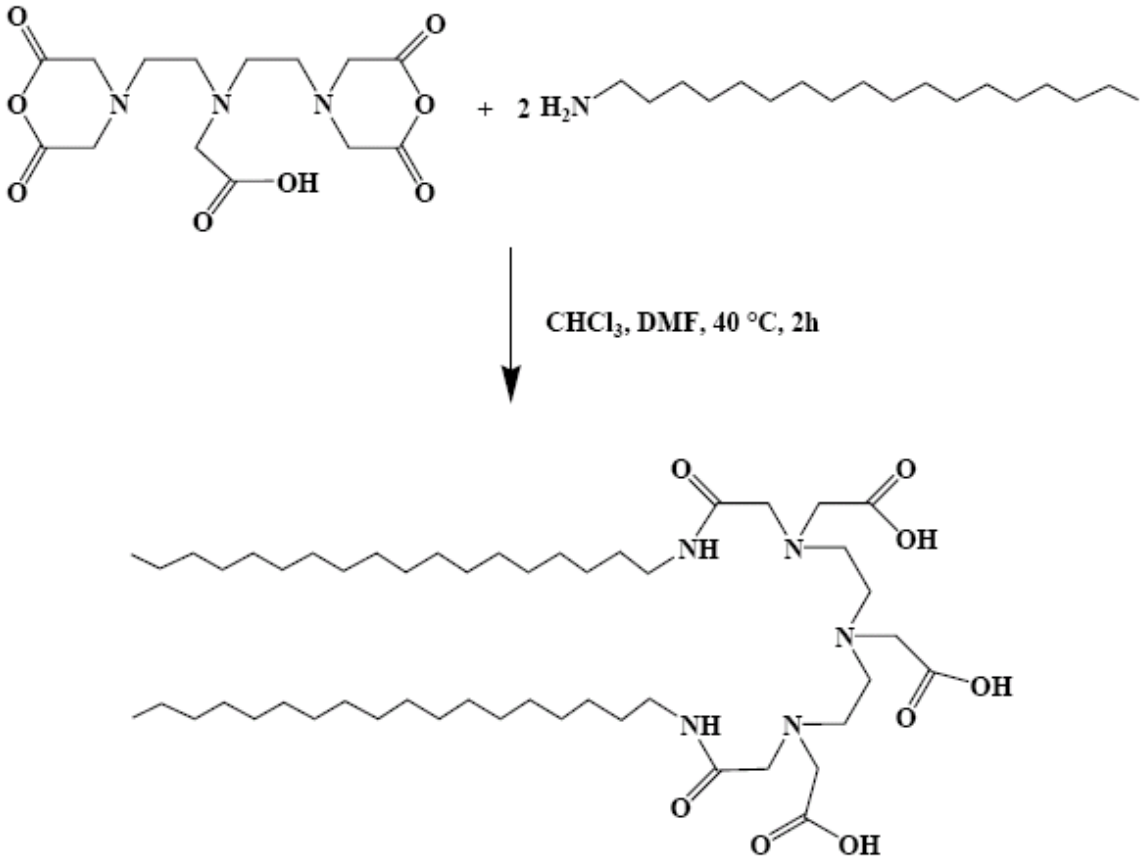

Scheme 4. Synthesis of diethylenetriamine pentaacetic acid bis-stearylamide (DTPA-DSA)

Diethylenetriamine pentaacetic acid (DTPA) dianhydride (1.965 g; 5.5 mmol, Aldrich) was dissolved in 200 ml of anhydrous DMF (ACROS) at 40 °C. Octadecylamine (stearyl amine, SA, Aldrich) (2.695 g; 10 mmol) was dissolved in 250 ml of anhydrous $CHCl_3$ (ACROS) and added dropwise at 40 °C. The reaction mixture was stirred at 40 °C 2h, then cooled down and stored overnight at 4 °C. The white precipitate was filtered off, washed with acetone (0.5 L, Fisher) dried, then heated in boiling absolute ethanol (1 L, Fisher) and filtered hot. The filtrate was cooled down and the precipitate was filtered off and air-dried. The resulting crude product was boiled in chloroform for 3 h. After filtration the solid was stirred in 1 L of boiling water 3h. The dry residue was crystallized from 2 L of absolute ethanol. The white crystals were filtered off and dried under vacuum. Obtained 3.22 g of DTPA-DSA (71.8 %). MALDI-TOF (895 $[M]^+$, 918 $[M+Na]^+$). ^1H NMR (500 MHz, CF_3COOD, 305 K, δ ppm, ref. CF_3COOH, 11.62 ppm): 4.58 (s, 4H, CH_2), 4.56 (s, 4H, CH_2), 4.18 (s, 2H, CH_2), 4.1 (m, 4H, CH_2), 3.8 (m, 4H, CH_2), 3.41 (t, 4H,

CH_2), 1.6 (m , 4H, CH_2), 1.3 (m , 60H, CH_2), 0.9 (t, 6H, CH_3). TLC ($CHCl_3$/MeOH/H_2O/CH_3COOH, 25/15/4/2, v/v) R_f = 0.4.
DTPA-DSA was used for Gd^{3+} loading.

Synthesis of DTPA-DSA-Gd monohydrate.

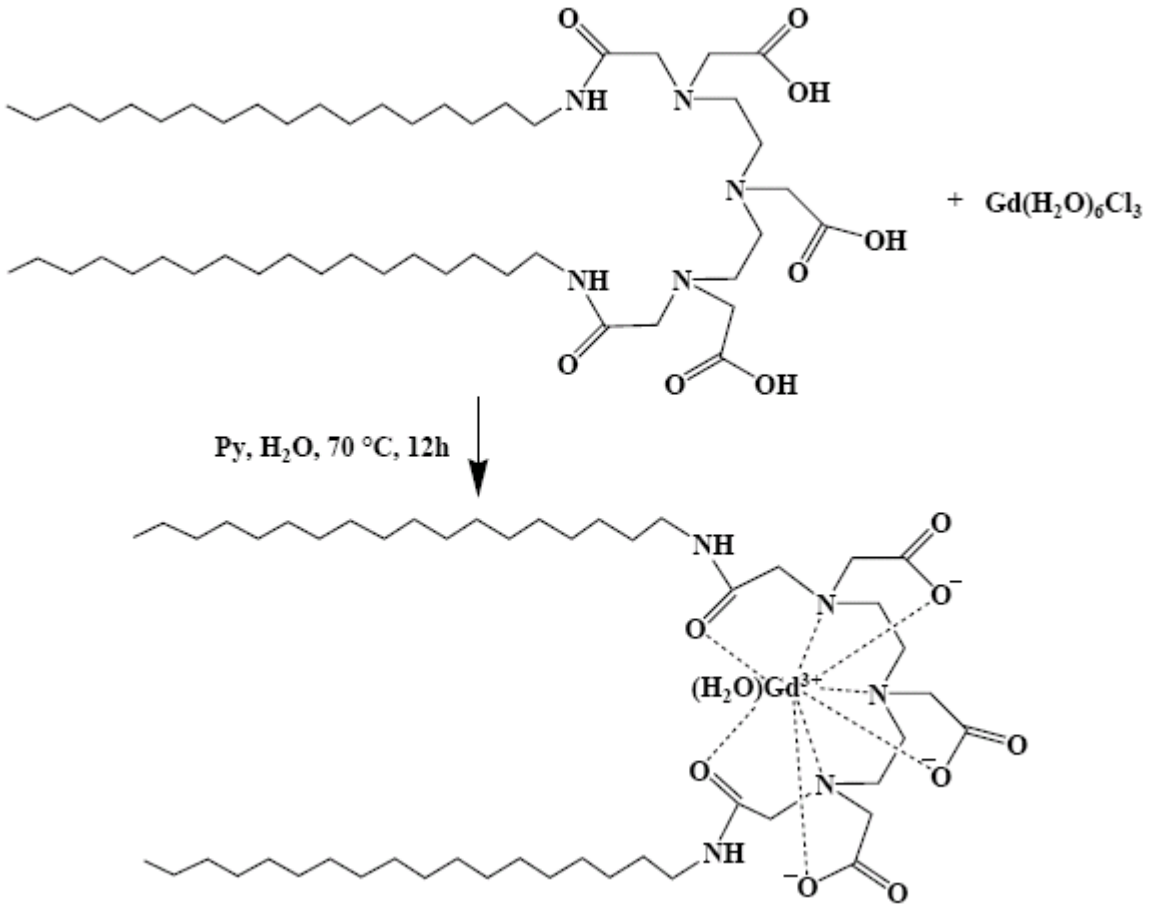

Scheme 5. Synthesis of DTPA-DSA-Gd monohydrate

Gadolinium (III) chloride hexahydrate (408.3 m g 1.1 mmol, Aldrich) was dissolved in water (1 mL) and added to a mixture of DTPA-SA (896.3 m g, 1 mm ol) and dry pyridine (30 mL, ACROS). The reaction m ixture was stirred overnight at 70 °C. Th e volatiles were evapora ted under reduced pressure. The residue was heated at reflux in ethanol (0.5 L) 1h. Then most of the solvent was evaporated until 100 m L volume and the product was precipitated into water (1 L). The solid greenish crystals were filtered off, washed with water (3x300 m L) a nd dried in vacuum. The absence of free gadolinium was checked with xylenol orange indicator. Yield 890.1 mg (83.3%). MALDI-TOF 1091 $[M+Na]^+$.
DTPA-DSA-Gd monohydrate is to be incorporated into the lipid nanoparticles shell for MRI and multimodal imaging.

2.2.2. Synthesis of core components

Synthesis of 5-Androsten-17*β*-Boc-amino-3*β*-yl Oleate (BOC-CE-OA, Scheme 6)

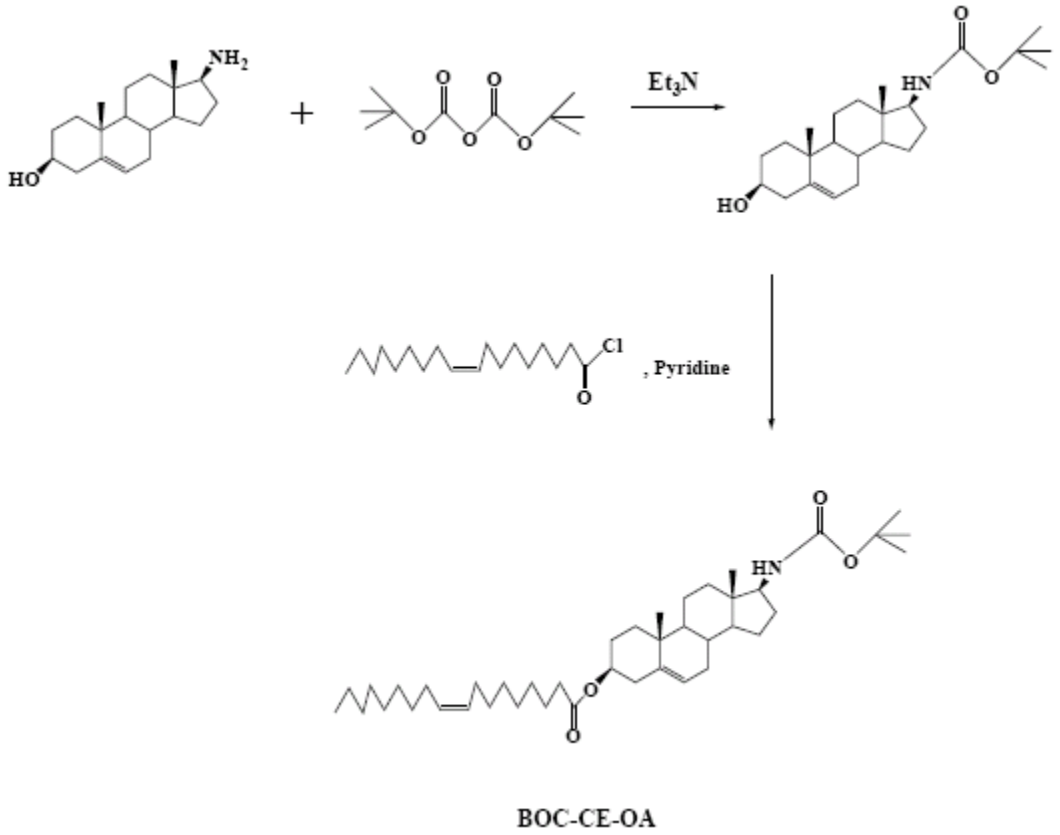

Scheme 6. Synthesis 5-Androsten-17*β*-Boc-amino-3*β*-yl Oleate (BOC-CE-OA)

Synthesis of 5-Androsten-17*β*-Boc-amino-3*β*-ol (BOC-CE)

Di-*tert*-butyl dicarbonate (420 g, 1.90 mmol) was added to a solution containing 5 androsten-17*β*-amino-3*β*-ol (475 mg, 1.64 mmol) and triethylamine (0.27 mL, 1.94 mmol) in dichloromethane (50 mL). The reaction mixture was stirred at room temperature for 2 days. Evaporation of the solvent gave a white residue. This crude product was purified by silica gel column chromatography (30% ethyl acetate in hexanes) to give BOC-CE as a white solid in 95% yield (610 mg, 1.57 mmol). Mp: 168-172 °C; exact mass calcd: 389.3; found by ESI-MS: 390.4 (MH+). Anal. Calcd for $C_{24}H_{39}NO_3$: C, 73.99; H, 10.09; N, 3.60. Found: C, 73.52; H, 10.39; N, 3.19. ^{1}H NMR ($CDCl_3$): δ 5.34 (m, 1H, 6-H), 4.42 (brs, 1H, N-H), 3.53 (m, 2H, 3-H + 17-H), 2.27 (m, 2H), 2.17-1.92 (m, 2H), 1.90-1.70 (m, 3H), 1.69-1.49 (m, 6H), 1.48-1.32 (m, 3H), 1.44 (s, 9H for *tert*-butyl), 1.31-1.15 (m, 2H), 1.15-0.95 (m, 2H), 1.00 (s, 3H, 19-CH_3), 0.67 (s, 3H, 18-CH_3); ^{13}C NMR ($CDCl_3$): δ 156.2, 141.1, 121.5, 79.2, 71.9, 60.5, 53.0, 50.4, 42.8, 42.5, 37.5, 37.2, 36.8, 32.3, 31.8, 31.7, 29.0, 28.6, 28.6, 28.6, 23.7, 20.9, 19.6, 12.0.

Synthesis of 5-Androsten-17β-Boc-amino-3β-yl Oleate (BOC-CE-OA)

Oleoyl chloride (710 mg, 2.35 mmol) was slowly added into a 20 mL pyridine solution of BOC-CE (610 mg, 1.57 mmol). After 2 h, the reaction mixture was poured into 40 mL of icewater. It was filtered and washed with water three times to give a crude residue. This crude product was then chromatographed on silica column with 10% ethyl acetate in hexanes to afford the title compound as sticky solid in 60% yield (615 mg, 0.94 mmol). Exact mass calcd: 653.5; found by ESI-MS: 654.6 (MH^+). Anal. Calcd for $C_{42}H_{71}NO_4$: C, 77.13; H, 10.94; N, 2.14. Found: C, 77.35; H, 11.41; N, 1.76. 1H NMR ($CDCl_3$): δ 5.32 (m, 3H, 6-H + 2 x vinyl-H of oleate), 4.58 (m, 1H, 3-H), 4.41 (brs, 1H, N-H), 3.52 (m, 1H, 17-H), 2.28 (m, 4H), 2.17-1.70 (m, 10H), 1.61 (m, 8H), 1.50-1.38 (m, 2H), 1.43 (s, 9H for *tert*-butyl), 1.37-0.95 (m, 23H), 1.00 (s, 3H, 19-CH_3), 0.85 (t, 3H, terminal CH_3 of oleate), 0.65 (s, 3H, 18-CH_3); ^{13}C NMR ($CDCl_3$): δ 173.3, 139.4, 130.1, 129.9, 122.4, 78.1, 73.7, 60.5, 52.8, 50.2, 42.7, 38.3, 37.1, 37.0, 36.8, 34.8, 32.2, 32.1, 31.7, 29.9, 29.8, 29.7, 29.5, 29.5, 29.3, 29.3, 29.2, 29.2, 28.9, 28.6, 28.6, 28.6, 27.9, 27.4, 27.3, 25.2, 23.7, 22.8, 20.7, 19.5, 14.3, 11.9.

2.2.3. Assembling the nanoparticles

To assemble nanoparticles, we combined chloroform solutions of PEGylated lipids (1,2-distearoyl-*sn*-glycero-3-phosphoethanolamine-N-[methoxy(polyethylene glycol)-1000]), metal-chelating lipids (1,2-dioleoyl-*sn*-glycero-3-[(N-(5-amino-1-carboxypentyl)iminodiacetic acid)succinyl]), cholesterol esters and lipids conjugated with imaging agents. Excess of the PEGylated lipids (70-80%) provided the formation of lipid monolayer shell to avoid creation of a bilayer shell that would significantly increase the size of the lipid particles. 20% of DOGS-NTA containing lipids allowed to maximize the density of metal chelating groups and, consequently, the density of ligands bound to the nanoparticles and the strength of His_6-tagged ligand interaction with the metal chelating groups[8]. 10-15% of cholesterol esters were sufficient to completely fill out the interior space of the nanoparticles that served as the nanoparticles core. When the content of the core lipids was increased the lipid precipitation was observed indicating that nanoparticle core can accommodate a limited amount of cholesterol esters molecules. Chloroform was removed with argon stream and lipid film additionally dried under vacuum for 3hr. Lipids were hydrated under argon with hot (65-80 °C) HBS buffer (10 mM HEPES, 140 mM NaCl) by intermitted vortex and were cooled down in a water bath to room temperature. Micelle suspension was filtrated through a 0.2 μm mini filter (Sterlitech) and kept under argon at 4 °C.

2.2.4. The nanoparticle size measurements

To vary the particles size we used core lipids of different nature. The nanoparticles without core were used as control. The size of the resulting nanoparticles was determined by dynamic light scattering (Table 1 and Fig.1). The particles with cholesterol core had largest size (up to 20 nm) due to cholesterol molecule intercalation between the shell lipids. After addition of fatty acid moiety to cholesterol molecule the nanoparticles size was decreased due to strong hydrophobic interaction between core molecules. Nanoparticles containing cholesterol ester derivatives that formed intermolecular hydrogen bonds had a smallest size, which approximately equal to the size of antibodies, with narrow size distribution pattern.

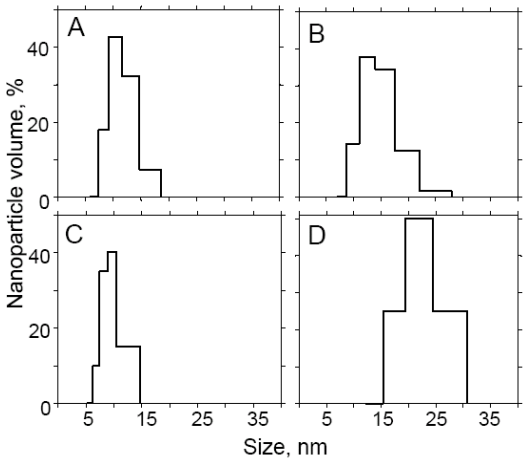

Figure 1. *Size distribution of nanoparticles from Dynamic Light Scattering analysis (A, B, C, D – see Table 1)*

Table 1. Dependence of the lipid nanoparticles size on the core content

Name of nanoparticles	PEGylated lipid, %	Ni-NTA lipid, %	Core lipid, name and %	Size, nm
A 78		22	N/A	10.1±5.4
B	70	20	10 (cholesterol ester) 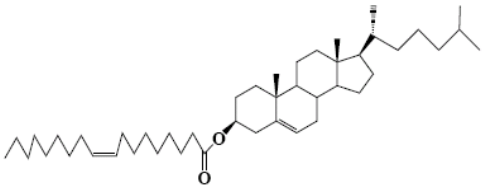	12.8±7.3
C 70		20	10 (BOC-CE-OA) 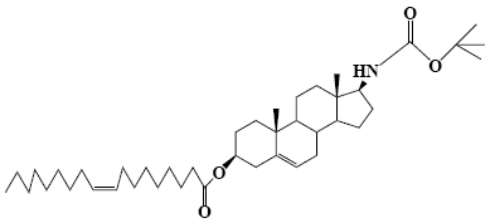	8.4±3.4
D 70		20	10 (cholesterol) 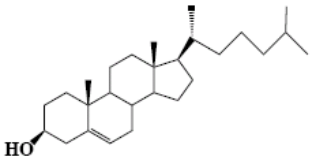	19.7±9.1

2.2.5. Formation of fluorescent nanoparticles

To endow lipid nanoparticles with fluorescent properties the porphyrin-based fluorophore, i.e. pyropheophorbide *a* was utilized. The pyropheophorbide *a* is excited by near infrared light that easily penetrates into live tissues and can be used for imaging and killing of breast cancer cells *in vivo*. To make fluorescently labeled lipid nanoparticles we used two different strategies: lipid-conjugated fluorochrome was introduced into either core or shell lipids of the nanoparticles. Pyro-CE-OA that contains cholesterol oleate moiety has been included in the nanoparticle core while pyropheophorbide *a* conjugated with phosphatidylethanolamine (Pyro-PE) have been incorporated into the shell.

Before the assembly of the nanoparticles each fluorescent conjugate was dissolved in chloroform, and absorption of the solution was measured at 410 nm. Using the extinction coefficient for Pyro that was determined as we described early ($\varepsilon = 110{,}000\ M^{-1}cm^{-1}$)[7] we were able to calculate the concentration of the Pyro conjugate solutions. To avoid self-quenching process we included only 3 mol% of fluorochrome molecules into the nanoparticle. To core formation we used acylated amino-cholesterol (BOC-CE-OA) ester that formed smallest NP (diameter 8 nm, Fig. 1, Tab. 1). For comparison reasons, we have also utilized DiI (Invitrogen), a lipophilic analog of an FDA approved carbocyanine dye, that was introduced into the lipid shell.

2.2.6. Functionalization of the nanoparticles with His_6-tagged protein

Elevated expression of cell surface receptors such as HER-2/neu[9-16] or integrin αvβ3 or α5β1 have been noted on breast cancer cells that is essential to tumorigenesis[17]. Every so often intrinsic affinity of receptor to natural ligands or peptidomimetics is relatively low ($\approx 10^4$ L/M). Nevertheless we expect strong multivalent binding of the nanoparticles carrying ligands the specific receptors on breast cancer cells according to our previous data[18]. To test this hypothesis we used a model cell-nanoparticle system, which consists from nanoparticles functionalized with ICAM-1 ligand that recognized αLβ2 integrin and CER-43 human T cell line over-expressing the latter molecule on the cell surface. We expressed soluble recombinant ICAM-1 protein containing His_6-tag on the C-end of the molecule in Drosophila cell system and purified by affinity chromatography on monoclonal antibody against human ICAM-1 (HB9580, ATCC) (data not shown).

The nanoparticles functionalization included two steps. (i) To load NTA-DOGS shell lipids with Ni^{2+} a Bio-Rad mini column with cut off 6 kDa was equilibrated with 100 mM $NiSO_4$, and the nanoparticles solution at total lipid concentration of 5 mM was passed through the column to exchange the buffer. After 30 min of incubation unbound Ni^{2+} ions were removed by an additional cycle of gel filtration on the Bio-Rad mini column pre-equilibrated with HBS buffer. (ii) The resulting nanoparticles containing imaging agent (see section 2.2.5.) at total lipid concentration around 5 mM were mixed with equal volume of the His_6-tagged recombinant ICAM-1 at different concentrations (up to 100 μM). The mixture was incubated at room temperature during 10 min and desirable amount of PBS with 1% BSA was added.

2.2.7. Analysis of the nanoparticle specificity by Flow Cytometry

To analyze binding specificity of ICAM-1-NPs two different NPs were used: (i) NP containing fluorescent lipid conjugate in the core (ICAM-1-NP-Pyro-CE-OA) and (ii) NP with fluorescent lipids in the shell (ICAM-1-NP-Pyro-PE). The NP were added to CER-43 cells in PBS buffer containing 1mM Ca^{2+}, 1 mM Mg^{2+} and 1% BSA. About 10 nmol lipid was used per 200,000 cells. Control cells were stained with unloaded particles. The cells were incubated for 3hr at 37 °C, washed free of unreacted reagents and analyzed by Flow Cytometry. As shown in **Figure 2A** and **B** the loaded nanoparticles specifically stain CER43 cells without significant background. The cells incubated with ICAM-1-NP-Pyro-PE stained more intensely (higher MFI) than ICAM-1-NP-Pyro-CE-OA treated cells.

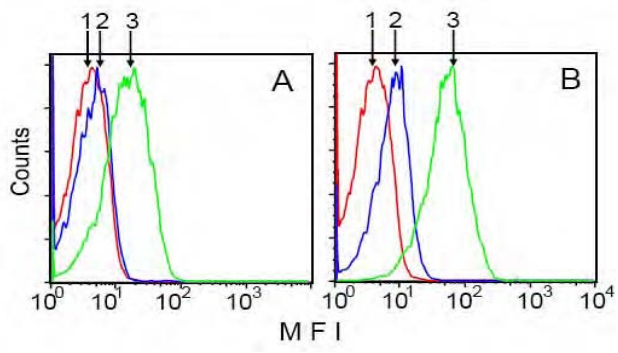

Figure 2. *Binding of ICAM-1-NP (3) to CER-43 cells expressing alphaLbeta2 integrins on the surface that specifically recognize ICAM-1 molecule: (**A**) ICAM-1-NP-Pyro-CE-OA and (**B**) ICAM-1-NP-Pyro-PE. Untreated cells (1) and cells incubated with plain NP, i.e., untargeted nanoparticles (2) were used as negative controls. Fluorescence was excited at 633 nm and emission was collected at 675 nm.*

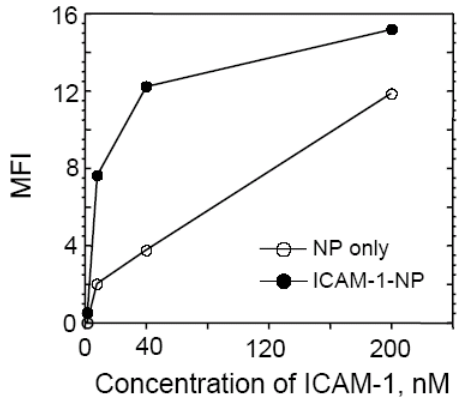

Figure 3. *The binding of ICAM-1-NP-Pyro-CE-OA to CER-43 cells upon concentration of ICAM-1 is shown. Cells incubated with untargeted nanoparticles were used as a negative control.*

The staining was highly sensitive ($K_{avidity}$ ~ 8 nM) presumably due to multivalent nature of ICAM-1-NP (**Fig. 3**).

To understand better the difference in the staining pattern of NP containing different fluorescent conjugates we investigated changes of the cell MFI as function of time (**Fig. 4A** and **B**). As clearly evident from **Figure 4** the fluorescence of the cells stained with ICAM-1-NP-Pyro-PE dramatically increased while fluorescence of the cells incubated with ICAM-1-NP-Pyro-CE-OA stayed constant. We suggest that shell-associated fluorescent lipids can exchange with cell membrane lipids allowing accumulation of fluorochrome in the cell membrane of target cells thus increasing intensity of cell staining[19]. Pyro-CE-OA conjugate lipids have much lower ability to accumulate in the cell membrane. Moreover, after releasing content of endocytosed NP in cytoplasm Pyro-CE-OA conjugate lipids can aggregate limiting cell fluorescence due to self-quenching.

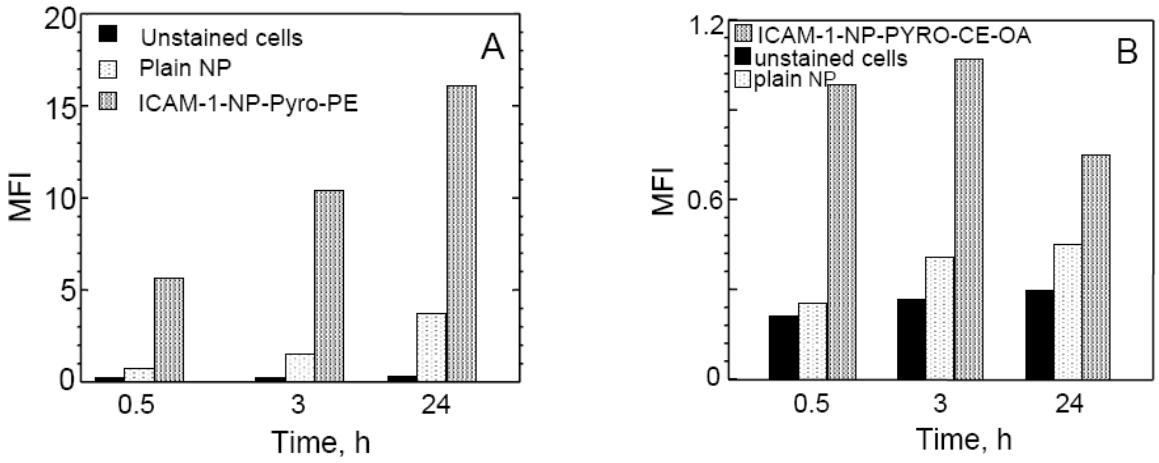

Figure 4. *Time course of the cell staining using different ICAM-1-NP is shown. CER-43 cells were incubated in the presence of ICAM-1-NP-Pyro-PE (**A**) or ICAM-1-NP-Pyro-CE-OA (**B**) for 30 min to 24 h. After repeated washing to remove free nanoparticles the cells were analyzed by Flow Cytometry.*

2.2.8. Fluorescent image analysis

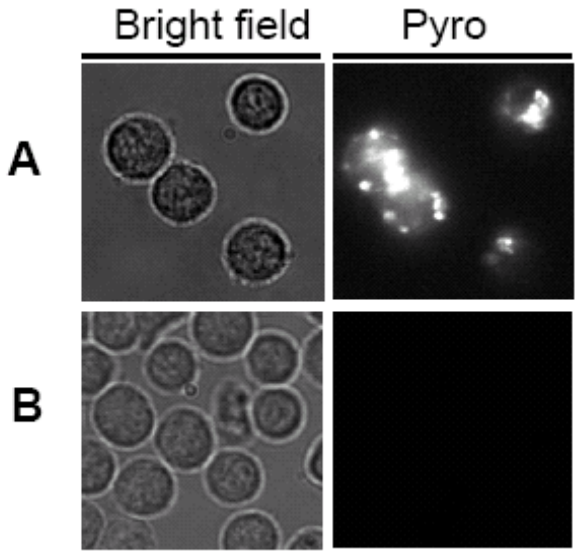

Figure 5. *Binding of ICAM-1-NP-Pyro-PE to the surface of live cells. CER-43 cells were stained with ICAM-1-NP-Pyro-PE for 3 hr at 37 °C. Plain NPs were used as a negative control. About 10 nmol of lipids was used per 200,000 cells. After washing procedure the samples were used for microscopy on a traditional wide field fluorescence microscope with Live Cell System. The probes near-infrared fluorescence were excited by Xenon Lamp at 620/60 nm and emission was collected with 700/75 nm band pass filter.*

The specificity of the ICAM-1-NP-Pyro-PE binding was also evident from the analysis of fluorescence images of CER-43 cells incubated with the NPs at 37 °C (**Fig. 5**). The binding of untargeted NPs to the CER-43 cells was not observed thus confirming specificity of the process (**Fig 5B**). Interaction of ICAM-1-NP-Pyro-PE with the surface of CER-43 cells leads to internalization of the NPs that is evident from punctate surface and intracellular staining (**Fig 5A**). The intensity of the staining and amount of internalized NP increased with time (data not shown). Thus, the imaging data confirm the NP targeting at the cell surface and subsequent receptor mediated uptake.
To support the above data we used ICAM-1-NP loaded with well-characterized lipophilic tracer DiI.

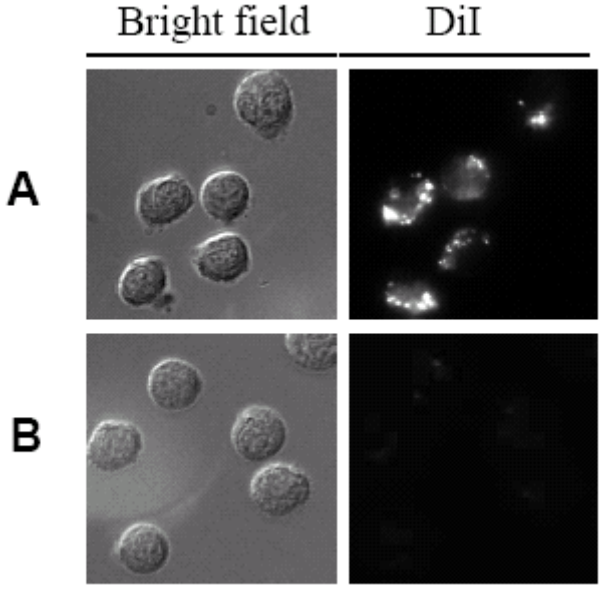

Figure 6. *CER-43 cells staining with DiI loaded ICAM-1-NP. CER-43 cells were stained with ICAM-1-NP-DiI as described in Figure 5. Samples were exited at 540/20 nm and emission was collected with D605/55 nm filter.*

It is weakly fluorescent in aqueous environment. However, it is highly fluorescent when incorporated into lipid membranes such as plasma, endosome and lysosome membranes. After incubation of the CER-43 cells with ICAM-1-NP-DiI the staining pattern, i.e., intensity, specificity and localization of the fluorescent probe, was similar to the fluorescence of the ICAM-1-NP-Pyro-PE treated cells (**Fig. 6**).

2.2.9. Design of the anti-p185$^{her2/neu}$ peptidomimetic

Peptidomimetic AHNP (FCDGFYACYM DV) is an exo-cyclic peptide that was rationally derived from the structure of the CDR-H3 loop of the antibody h4D5 (Herceptin). The peptide keep the most of the antibody functional activity *in vitro* and *in vivo* whereas the affinity of the peptide (~300 nM) far less then the affinity of the whole antibody (0.1 nM). The lipid-based NPs represent an ideal scaffold for the assembly of multivalent peptidomimetics with enhanced functional potential. [20]
We introduced three additional elements in the peptidomimetics design: (i) His_6-tag on the C-terminus end for binding with Ni^{2+}-NTA group of the NPs; (ii) repeated $(EAAAK)_4$ peptide

linker, forming alpha coil; (iii) short flexible linkers (GS and SG) between the elements (**Fig**. 7). The length of the alpha helical structure in the C-end of the designed peptidomimetics (AHNP-His) approximately equal the length of the PEG, which presumable have "brush" conformation on the NP surface[21]. Thus, introducing the alpha coil structure should increase accessibility of peptidemimetic binding site during recognition of Her2/neu on target cell surface.
The peptide was synthesized and purified by Bachem Americas Inc.

FCDGFYACYMDVGS*LAEAAAKEAAAKEAAAKEAAAKAAA*SGHHHHHH
Cys2-Cys8 bond

Figure 7. *Structure of the AHNP-His peptidomimetic*
Bold*: structure of binding site;*
Italic: amino acid sequence of alpha helical structure;
Underline*: His_6-tag*

2.2.10. Interaction of AHNP-His with Her2/neu presented on the surface of breast cancer cell line SKBR-3

To test AHNP-His for Her2/neu binding we chose SKBR-3 cell line that expressed around 10^6 receptor molecules on the cell surface. The cells were detached with Cellstripper buffer (Cellgro). After washing procedure the cells were resuspended in DPBS/1%BSA buffer containing various concentration of ANHP-His peptidomimetics and incubated for 30 min at 4 °C. Then cells were sequentially treated with mouse anti-His_6-tag antibody (PentaHis, Qiagen) and Alexa488 conjugated goat anti-mouse $F(ab')_2$ fragment. The peptide binding was analyzed by Flow Cytometry. As evident from **Fig. 8**, the affinity of the AHNP-His interaction with the receptor on the cell surface is much higher (>100 μM) then the affinity of the parental peptidomimetic measured by Biacore (350 nM) [22]. It has been shown that many of the peptidomimetics presumably form multimeric aggregates with poorly defined structures and low specificity[23]. Moreover, fusion AHNP with streptavidin results in faster dissociation rate constant then the parental AHNP peptide [20]. Addition of the peptide linker on the C-end of the peptidomimetic also can influence on the dissociation rate constant of AHNP-His - Her2/neu. In agreement with this, Pyro-NP conjugated with AHNP-His binds to the surface of SKBR-3 cells only slightly better (20%) then unloaded NPs even at 10 μM peptide concentration (data not shown).

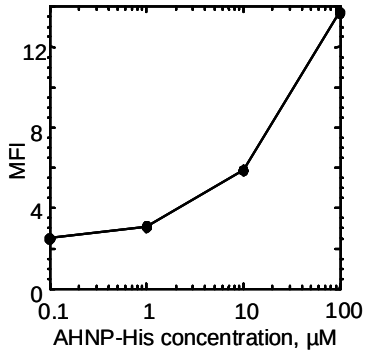

Figure 8. *Binding of the AHNP-His peptidomimetic to the surface of the human breast cancer cell line SKBR-3*

2.2.11. Conjugation of the NPs with HER2/neu-binding Affibody ligand

To increase specificity and sensitivity of targeting we decided to utilize anti-Her2 Affibody molecule, which is highly specific affinity ligand ($K_d \approx 50$ nM, MW ≈14 kDa) selected against the extra cellular domain of Her-2/neu [24]. The Affibody molecule (Affibody AB, Sweden) contains a unique cysteine at the C-terminus that can advantageously be used for direct conjugation.

To conjugate of the Affibody with fluorescent NPs we incorporated 25 mol% of maleimide-functionalized lipids (1,2-distearoyl-*sn*-glycero-3-phosphoethanolamine-N-[maleimide(polyethylene glycol)-2000], Avanti Polar lipids) in NPs composition.

The affibody molecules spontaneously generate tail-to-tail dimmers via a disulfide bridge between the C-terminal cysteines. Prior to coupling via Cys residue we incubated 150 µg Affibody in PBS buffer, pH 7.6 containing 20 mM DTT for 1 hour at room temperature under argon. Excess of DTT was removed by passage through the BioRad P 6 column and resulting solution was immediately mixed with 35 µl (5mM lipids) maleimide-functionalized NPs in coupling buffer (10 mM HEPES, 140 mM NaCl, pH 7.2). The reaction was incubated at 25 °C for 1 hour under argon and additional 10 min with 1 mM cysteine solution to blocking unreacted maleimide group.

The aliquots of NP coupled Affibody and control NPs treated with 1mM cysteine, as well as unmodified Affibody, were analyzed by reducing SDS-PAGE. The result obtained by PAGE is shown in **Fig. 9**, where the position of reduced Affibody, Affibody dimers and PEG2000-PE-conjugated Affibody are indicated. Although the probes were boiled with reducing SDS-PAGE sample buffer for 5 minute the bands of the Affibody dimer were observed in both unmodified and coupled Affibody samples. It is suggested that a part of the protein irreversibly aggregated and likely is not active.

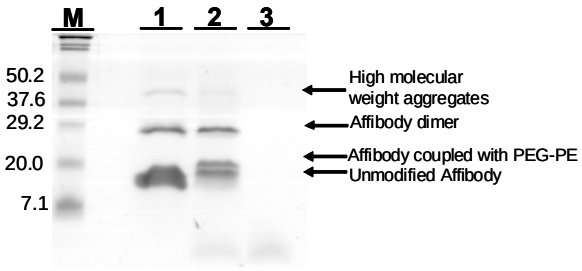

Figure 9. *SDS-PAGE analysis (18% gel, reducing conditions) of the NPs conjugated with the Affibody: unconjugated Affibody (line 1); the Affibody conjugated with PEG2000-PE of the NPs (line 2); uncoupled NPs (line 3)*

The coupled NPs were separated from free Affibody molecules by gel filtration. Elution profile of fluorescent NPs was monitored by spectrophotometrically, and concentration of the protein was evaluated with Bradford reagent. As evident from **Fig. 10**, a high proportion of the Affibody was coupled with NPs. The fractions containing NPs were collected, concentrated using Amicon Ultra Centrifugal Filter and kept under argon at 4 °C.

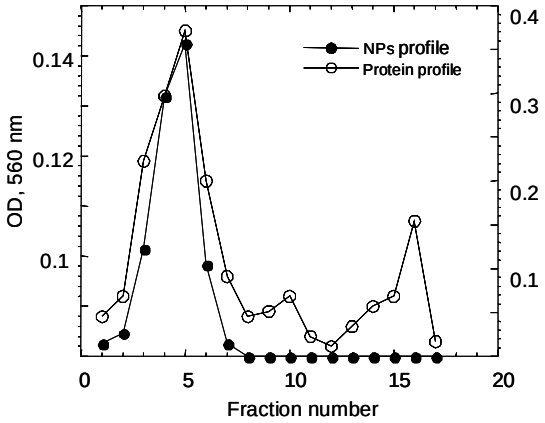

Figure 10. *Separation of NPs coupled from free Affibody molecules*

The conjugated NPs (5 nmol lipids) were incubated with stripped SKBR cells at 4 °C for 30 minutes. After washing procedure the cells were analyzed by Flow Cytometry. Binding of the NPs to the cell surface was not observed presumably due to aggregated state of the Affibody molecules.

2.2.12. NPs conjugation with 25-D1.16 Fab and analysis of binding specificity

Although a peptidomimetics and Affibodies with antibody like specificity seem to be very attractive due to small molecular weight and consequently cost of the production, their low specificity and/or poor stability often preclude usage of these ligands in clinical practice. We decided to use the recombinant Fab fragment of TCR-like antibody 25-D1.16 containing His_6-tag on C-terminal end to confirm the feasibility of the NPs as a targeting nanocarrier.
The recombinant Fab fragments of antibody 25-D1.16 recognizing pOV8 peptide from ovalbumin in association with H-2 K^b class I MHC were produced in *Drosophila melanogaster* cells and were successfully used as a targeting protein in composite immunotoxin[8,25].
To assemble the targeted NPs (Pyro-NP-Fab), 1 µl of Pyro-NPs (5mM lipids) with cholesterol oleate core were combined with 1 µg 25-D1.16 Fab and incubated for 10 minutes at room temperature. To test the ability of Pyro-NP-Fab to recognize pOV8-K^b proteins on the surface of live cells, mouse lymphoma cell line EL4 was pulsed with either cognate (pOV8) or irrelevant (VSV) peptide at 10^{-5} M for 1 h in complete culture medium. Cells were washed and then resuspended in 100 µl of culture media containing the Pyro-NP-Fab. Additional negative control included the cells incubated with unconjugated NPs. The samples were incubated at 37 °C for different time interval, and after washing procedure the cells were analyzed by Flow Cytometry on Beckman Coulter FACS analyser. The Pyro-NP-Fab specifically interacted with cells presenting pOV8-K^b molecules on the cell surface (**Fig. 11**). The specificity of staining increased with time. Thus, antibody Fab fragments conjugated with the Pyro-NPs can be successfully used to specific targeting of cancer cells.

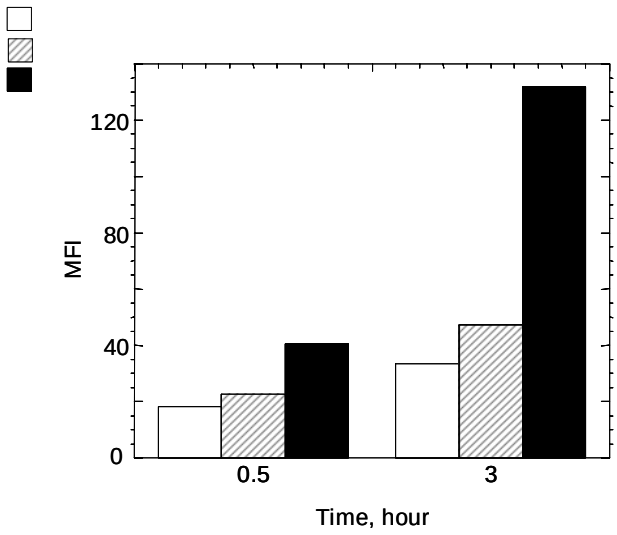

Figure 11. *Binding specificity of Pyro-NP-Fab. EL4 cells sensitized with peptide pOV8 (■) but not with VSV(▨) peptide were specifically stained with NPs conjugated with 25-D1.16 Fab. The cells incubated with unconjugated NPs (□) did not show specific staining.*

2.2.13. Influence of the core nature on NP stability

The introduction of cholesterol esters derivatives into hydrophobic core of the NPs will enable us to produce the particles of a smaller size. It has been shown that cholesterol esters are major constituents of the hydrophobic core of low-density lipoprotein particles[26] that are very stable in blood. It also has been shown that decreased core rigidity (transition temperature) reduces the NP blood residence time[27]. We hypothesize that cholesterol esters with high transition temperature could also significantly improve stability of the NPs at conditions close physiological.

To compare the stability of the NPs with different core we decided to find the dependence of the binding and functional activity of the targeting NPs on time at 37 °C in the presence of serum. As a ligand for targeting we chose the GL9- HLA-A2 complex, which was utilized in our previous work to compare binding specificity and functionality of the conjugated QDs[18].

HLA-A2 molecules containing a His_6-tag at the C-terminus were expressed and purified as described elsewhere[28]. Empty HLA-A2 (67 μM) was loaded with GL9 at peptide concentration of 100 μM overnight at 4 °C.

At first, we examined the ability of the fluorescent NPs conjugated with GL9-HLA-A2 (Pyro-NP-GL9-HLA-A2) to bind TCR on the surface of live CTL CER43 that recognizes GL9 in the context of HLA-A2. 1μl of NP solution (at 5 mM lipids) was mixed with 8 μl HBS buffer and 1.6 μl of GL9-HLA-A2 at concentration 50 μM. Mixture was incubated at room temperature for 10 min and 40 μl of RPMI with 10% FCS were added. $2x10^5$ CER-43 CTL were washed and then suspend in serum media containing the conjugated NPs. Control cells were loaded with unconjugated NPs. Staining procedure was done at 37 °C for 30 min. After washing procedure the samples were analyzed by Flow Cytometry. After conjugation with cognate GL9-HLA-A2 complex all NPs, which had distinct core, were bound to the surface of CER43 CTL albeit with different extent (**Fig. 12**). The cells incubated with Pyro-NP-GL9-HLA-A2 with cholesterol oleate core had the highest fluorescent intensity while

NPs with BOC-CE-OA core bound to the cells surface less effectively. This finding is in agreement with study the shelf-life of unconjugated NPs with different core. The NPs with BOC-CE-OA core started to precipitate after storage for 3 month at 4 °C. The NPs with cholesterol oleate core did not show any visible sign of precipitation even after 6 month (data not shown).

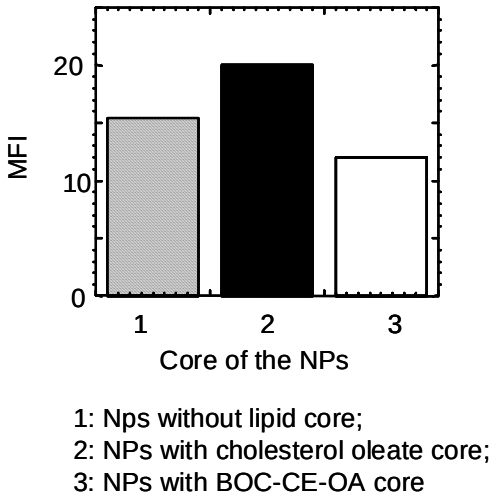

Figure 12. *Binding of Pyro-NP-GL9-HLA-A2 conjugates to the surface of live CER-43 CTL. GL9-HLA-A2 concentration was 1 μM; the binding was performed for 30 min at 37 °C. Although all Pyro-NP-GL9-HLA-A2 conjugates bind specifically to CER43 CTL, the conjugate with cholesterol oleate core demonstrates highest binding to the CTL (2), the NPs without core have intermediate ability to bind to the CTL surface (1), and the conjugate with BOC-CE-OA core have significantly reduced binding to live CER-43 CTL (3).*

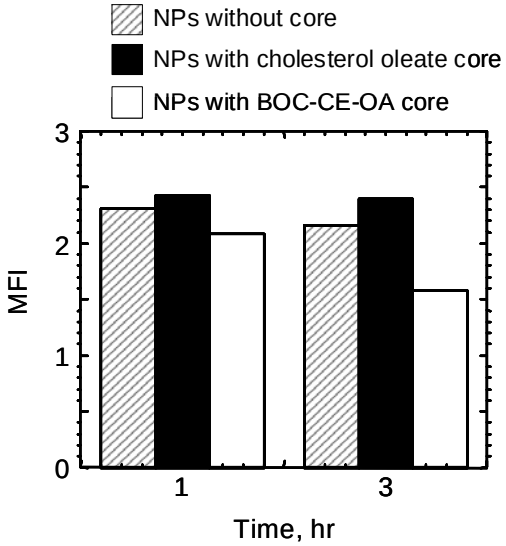

Figure 13. *Effectiveness of T cell response induced by Pyro-NP-GL9-HLA-A2 conjugates with different core was determined from maximal amplitude of Ca^{2+} flux and characterized by MFI.*

To confirm above data we compared the dependence of the functional activity of the Pyro-NP-GL9-HLA-A2 with different core on time after incubation at 37 °C. To answer the question, we used NPs that display cognate GL9-HLA-A2 to stimulate T cells with known specificity and monitor intracellular Ca^{2+} flux magnitude to measure stimulation.
CTL (10^7/ml) was loaded with Fluo 3 according to the manufacturer (Molecular Probes) instruction. The cells were washed free of unreacted dye and were resuspended in the assay buffer (Dulbecco's PBS containing 1 mM $CaCl_2$, 0.1 mM $MgCl_2$, 1 mM $CaCl_2$ 5mM glucose and 0.025% BSA) at 10^6/ml. 1 μl NP solution at 5 mM lipids was mixed with 70 pmol pMHC in total volume 10 μl during 10 min and prepared NP conjugates were incubated indicated time at 37 °C. After incubation the NP

conjugates were added to 1 ml of the CTL suspension and the samples were promptly analyzed on a Coulter Epics XL-MCL Flow Cytometer. The data collection was initiated as soon as possible (typically 20 s after mixing of the conjugates and CTL) following the background measurements. The data were analyzed with FlowJo software. After increasing incubation time from 1 to 3 hours the cells treated by NPs without core as well as NPs with BOC-CE-OA core demonstrated the decreasing of magnitude of Ca^{2+} flux albeit at different extent (**Fig. 13**). The NPs with cholesterol oleate core did not change the magnitude of the Ca^{2+} flux in CER-43 cells after increasing incubation time up to 3 hours at 37 °C. Moreover, the Pyro-NP-GL9-HLA-A2 with cholesterol oleate core effectively induced CTL response even after 24-hour incubation at 37 °C in culture media containing 10% serum (**Fig. 14**).
Thus, NPs with cholesterol oleate core have significantly improved stability at the conditions close to physiological ones. We expect that addition of this core component would help to build stable NPs with long circulation time and a lesser extravasation into the normal tissue.

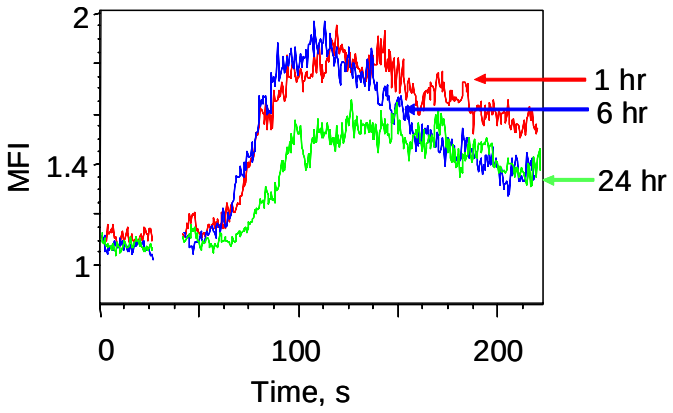

Figure 14. *Time-dependent changes in intracellular calcium concentration in CER43 CTLs induced by cognate Pyro-NP-GL9-HLA-A2 conjugate with cholesterol oleate core after preincubation of the NPs for indicated time at 37 °C in serum containing media.*

3. Key Research Accomplishments:

We have successfully synthesized fluorescent lipid conjugates that suitable for NIR imaging: pyropheophorbide *a* with phosphatidylethanolamine, pyropheophorbide *a* with cholesterol, and pyropheophorbide *a* with cholesterol oleate. We have also synthesized a lipid DTPA-Gd derivative for MRI and the nanoparticles core building block – an acylated cholesterolamine oleate.

We have assembled four different nanoparticles with core of different nature that affect on nanoparticles average size (from 8 nm for the smallest nanoparticles to 19 nm for the largest nanoparticles).

We have fabricated two kinds of fluorescent nanoparticles containing fluorescent lipids either in the core or in the shell.

We have conjugated the nanoparticles with three different ligands *via* C-terminal His_6-tag. The affibodies with C-terminal cysteine have been conjugated with the nanoparicles *via* maleimide-functionalized PEGylated lipids.

We have showed the specificity and measured sensitivity of the conjugated fluorescent nanoparticles using *in vitro* model system.

We have compared the stability of the nanoparticles with different cores at the conditions close to physiological ones.

4. Reportable Outcomes:

1. A.V. Popov. "Developing Molecular Probes and Nanoparticles for Imaging". University of Pennsylvania. March 5, 2009. Seminar for Research Assistant Professor position application.
2. Nadia Anikeeva, Yuri Sykulev, E. James Delikatny, and Anatoliy V. Popov. (2009) "Lipid-Based Nanoparticles for Targeted Delivery of Imaging Agents into Breast Cancer Cells and Cytotoxic T lymphocytes." The 3rd International Congress of Nanobiotechnology & Nanomedicine in San Francisco, June 22-24, 2009 Session Abstracts & Proceedings Table of Contents, T-A-6 AB PR. (Oral presentation, speaker A.V. Popov).
3. A.V. Popov, T.M. Mawn, S. Kim, G. Zheng, and E.J. Delikatny. "Design and Synthesis of Phospholipase C and A_2-Activatable Near Infrared Fluorescent Smart Probes". J. Amer. Chem. Soc. (Submitted)
4. A.V. Popov, N.N. Anikeeva, E.J. Delikatny and Yu. Sykulev. "Lipid-Based Nanoparticles for Targeted Delivery of Near Infrared Fluorescing Agents into Breast Cancer Cells and Cytotoxic T lymphocytes." Nano Letters. (In preparation)

5. Conclusion:

We have successfully been able to produce lipid-based targeted nanoparticles suitable for NIR imaging. Most materials used to produce the nanoparticles are biodegradable and are approved or about to be approved for clinical applications. The introduction of cholesterol ester into the hydrophobic core of the nanoparticles generates the particles of a small size and great stability at the conditions close to physiological ones. The self-assembling method to incorporate targeting agents into the nanoparticles bypasses any chemical modifications and preserves the targeting molecule functional activity. The modular organization of the proposed technology enables a combinatorial approach in which a repertoire of protein ligands can be utilized in conjugation with series of imaging agents coupled with lipids to yield a new generation of multifunctional targeting nanocarriers.

6. References:

1 Alexis, F., Rhee, J.- W., Richie, J. P., Radovic-Moreno, A. F., Langer, R. & Farokhzad, O. C. New frontiers in nanot echnology for can cer treatment. *Urol. Oncol.: Semin. Orig. Invest.* **26**, 74-85 (2008).

2 Cho, K., Wang, X., Nie, S., Chen, Z. & Shin, D. M. Therapeutic Nanoparticles for Drug Delivery in Cancer. *Clin. Cancer Res.* **14**, 1310-1316 (2008).

3 Torchilin, V. P. PEG-ba sed micelles as carrier s of contrast agents for different im aging modalities. *Adv. Drug Delivery Rev.* **54**, 235-252 (2002).

4 Allen, T. M. Ligand-targeted therapeutics in anticancer therapy. *Nat. Rev. Cancer* **2**, 750-763 (2002).

5 Bawarski, W. E., Chidlowsky, E., Bhara li, D. J. & Mousa, S. A. Em erging nanopharmaceuticals. *Nanomedicine* **4**, 273-282. (2008).

6 Heikela, M., Vattulainen, I. & Hyvonen, M. T. Atom istic sim ulation studies of cholesteryl oleates: model for the core of lipoprotein particles. *Biophys. J.* **90**, 2247-2257 (2006).

7 Popov, A. V., Mawn, T. M., Ki m, S., Zheng, G. & Delikatny, E. J. Design and Synthesis of Phospholipase C and A $_2$ -Activatable Near In frared Fluorescent Sm art Probes. *J. Am. Chem. Soc.*, (Submitted).

8 Anikeeva, N., Mareev a, T., Liu, W. & Sykul ev, Y. Can oligom eric T-cell recep tor be used as a tool to det ect v iral p eptide epito pes on infected cells ? *Clin. Immunol. (Amsterdam, Neth.)* **130**, 98-109 (2009).

9 Ciampa, A. & Khan, A. HER-2/neu status in breast cancer: "to FISH or not to FIS H". *Recent Res. Dev. Hum. Pathol.* **1**, 229-236 (2003).

10 Dhesy-Thind, B., Pritchard, K. I., Messers mith, H., O' Malley, F., Elavathil, L. & Trudeau, M. HER2/neu in system ic therapy for wom en with breas t cancer: a system atic review. *Breast Cancer Res. Treat.* **109**, 209-229 (2008).

11 Estevez, L. G. & Seidm an, A. D. HER2-positive breast cancer: incidence, prognosis, and treatment options. *Am. J. Cancer (Auckland, N. Z.)* **2**, 169-179 (2003).

12 Ferretti, G., Felici, A., Papaldo, P., Fabi, A. & Cognetti, F. HER2/neu role in breast cancer: from a prognostic foe to a predictive friend. *Curr Opin Obstet Gynecol* **19**, 56-62. (2007).

13 Lipton, A., De mers, L., Leitzel, K., Ali, S. M., Neumann, R., Price, C. P. & Carney, W . P. Circulating HER2/neu: clinical utility. *Biomarkers Breast Cancer*, 235-265 (2006).

14 Meric, F., Hung, M.-C., Hortobagyi Gabriel, N. & Hunt Kelly, K. HER2/neu in the management of invasive breast cancer. *J Am Coll Surg* **194**, 488-501. (2002).

15 Roh, H., Pi ppin, J. A., Green, D. W., Bos well, C. B., Hi rose, C. T., Mokadam , N. & Drebin, J. A. HER2/neu antisense ta rgeting of hum an bre ast carcinom a. *Oncogene* **19**, 6138-6143. (2000).

16 Vadgama, J., W u, Y. & Mehta, M. HER2/neu over expression in breast cancer: m ethods of detection and therap eutic im plications. *Mol. Cell. Pathol. Cancer Prog. Prognosis*, 327-358 (2006).

17 Liapis, H., Flath, A. & Kitazawa, S. Integr in alpha V beta 3 expression by bone-residin g breast cancer metastases. *Diagn Mol Pathol* **5**, 127-135. (1996).

18 Anikeeva, N., Lebedeva, T., Clapp, A. R., Go ldman, E. R., Dustin, M. L., Mattoussi, H. & Sykulev, Y. Quantum dot/peptide-MHC bi osensors reveal strong CD8-dependent

cooperation between self and viral antigens that augment the T cell response. *Proc. Natl. Acad. Sci. U. S. A.* **103**, 16846-16851 (2006).

19 Park, J. S., Han, T. H., Lee, K. Y., Han, S. S., Hwang, J. J., Moon, D. H., Kim, S. Y. & Cho, Y. W. N-acetyl histidine-conjugated glycol chitosan self-assembled nanoparticles for intracytoplasmic delivery of drugs: Endocytosis, exocytosis and drug release. *J. Controlled Release* **115**, 37-45 (2006).

20 Masuda, K., Richter, M., Song, X., Berezov, A., Masuda, K., Murali, R., Greene, M. I. & Zhang, H. AHNP-streptavidin: A tetrameric bacterially produced antibody surrogate fusion protein against p185her2/neu. *Oncogene* **25**, 7740-7746 (2006).

21 Lee, H., de Vries, A. H., Marrink, S.-J. & Pastor, R. W. A Coarse-Grained Model for Polyethylene Oxide and Polyethylene Glycol: Conformation and Hydrodynamics. *J. Phys. Chem. B* **113**, 13186-13194 (2009).

22 Berezov, A., Zhang, H.-T., Greene, M. I. & Murali, R. Disabling ErbB Receptors with Rationally Designed Exocyclic Mimetics of Antibodies: Structure-Function Analysis. *J. Med. Chem.* **44**, 2565-2574 (2001).

23 Timmerman, P., Barderas, R., Desmet, J., Altschuh, D., Shochat, S., Hollestelle, M. J., Hoeppener, J. W. M., Monasterio, A., Casal, J. I. & Meloen, R. H. A Combinatorial Approach for the Design of Complementarity-determining Region-derived Peptidomimetics with in Vitro Anti-tumoral Activity. *J. Biol. Chem.* **284**, 34126-34134 (2009).

24 Wikman, M., Steffen, A. C., Gunneriusson, E., Tolmachev, V., Adams, G. P., Carlsson, J. & Stahl, S. Selection and characterization of HER2/neu-binding affibody ligands. *Protein Eng., Des. Sel.* **17**, 455-462 (2004).

25 Mareeva, T., Wanjalla, C., Schnell, M. J. & Sykulev, Y. A novel composite immunotoxin that suppresses rabies virus production by the infected cells. *J. Immunol. Methods* **353**, 78-86 (2010).

26 Hevonoja, T., Pentikainen, M. O., Hyvonen, M. T., Kovanen, P. T. & Ala-Korpela, M. Structure of low density lipoprotein (LDL) particles: Basis for understanding molecular changes in modified LDL. *Biochim. Biophys. Acta, Mol. Cell Biol. Lipids* **1488**, 189-210 (2000).

27 Alexis, F., Pridgen, E., Molnar, L. K. & Farokhzad, O. C. Factors Affecting the Clearance and Biodistribution of Polymeric Nanoparticles. *Mol. Pharmaceutics* **5**, 505-515 (2008).

28 Anikeeva, N., Lebedeva, T., Sumaroka, M., Kalams, S. A. & Sykulev, Y. Soluble HIV-specific T cell receptor: expression, purification and analysis of the specificity. *J. Immunol. Methods* **277**, 75-86 (2003).

7. Appendices.

A.V. Popov, T.M. Mawn, S. Ki m, G. Zheng, and E.J. Delikatny. “Design and S ynthesis of Phospholipase C and A $_2$-Activatable Near Infrared Fluores cent Smart Probes”. J. Amer. Chem. Soc. (Submitted)

Design and Synthesis of Phospholipase C and A_2-Activatable Near Infrared Fluorescent Smart Probes

Anatoliy V. Popov,*[,†] Theresa M. Mawn,[†] Soungkyoo Kim,[†] Gang Zheng,[†,‡] and E. James Delikatny[†]

[†]*University of Pennsylvania, Department of Radiology, Philadelphia PA, 19104, USA, and* [‡]*University of Toronto, Department of Medical Biophysics, Toronto ON, M5G 1L7, Canada*

RECEIVED DATE (automatically inserted by publisher); E-mail: avpopov@mail.med.upenn.edu

Phospholipases (PLs) are ubiquitous enzymes that perform a number of critical regulatory functions. They catalyze phospholipid breakdown and are categorized as A_1, A_2 (PLA_2), C (PLC) and D (PLD) based on their site of action[1] (Figure 1).

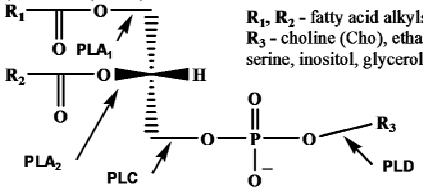

Figure 1. Phospholipase-mediated cleavage sites.

Since PLA_2 is elevated in a number of diseases (e.g. prostate and breast cancer, rheumatoid arthritis, etc)[2] we have chosen to develop probes that distinguish PLA_2 from other PLs. In addition, since increased PLC is detected in melanoma, ovarian and breast cancers and PLC has been implicated in maintaining the high levels of phosphocholine (PC) and phosphoethanolamine (PE) characteristic of many human tumors[3], we are also developing probes to specifically detect the actions of this enzyme.

The primary focus of this work is to develop methods to investigate the expression and activity of PLs *in vivo* in mammals. The above diseases can be detected, monitored and in some cases treated using soft tissue penetrating near infrared (NIR) light.[4] As a result we are employing optical imaging using NIR fluorophores (NIRF).

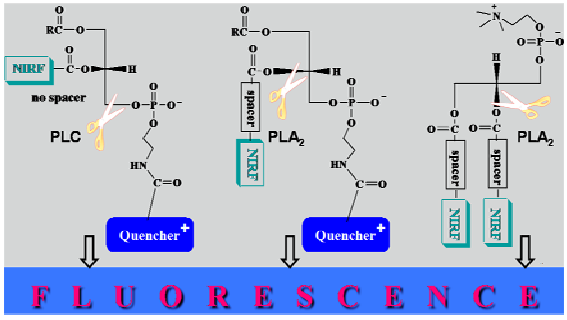

Figure 2. Design of NIRF-bearing PLC- and PLA_2-cleavable self quenched phospholipids.

Our approach is to design self-quenching reporter probes that release fluorescent moieties only upon cleavage with PLA_2 or PLC. The structures of these smart probes are depicted in Figure 2. The hypothesis is that a bulky porphyrin moiety attached at the *sn*2-position without a spacer would sterically hinder PLA_2 activity while leaving open the PLC cleavage site, whereas incorporation of spacers of different length will make the C-O bond at the *sn*2-position accessible for PLA_2 mediated hydrolysis. We have chosen Pyropheophorbide *a* (Pyro, **1**, λ_{abs} = 675 nm, λ_{em} = 725 nm) [5] as a NIRF. For quenchers, we employ either the positively charged Black Hole Quencher-3 (BHQ-3)[5] attached to the head group of the phospholipid or another neutral Pyro moiety at the *sn*1-position.

Scheme 1. Synthesis of Pyro-PtdEtn-BHQ (**4**), PyroC_{12}-PtdEtn-BHQ (**7**) and PyroC_6-PyroC_6-PtdCho (**10**) and structures for comparison of commercially available self-quenched PLA_2-sensitive green fluorescent phospholipid probes PED6 (**11**) and B7701 (**12**).

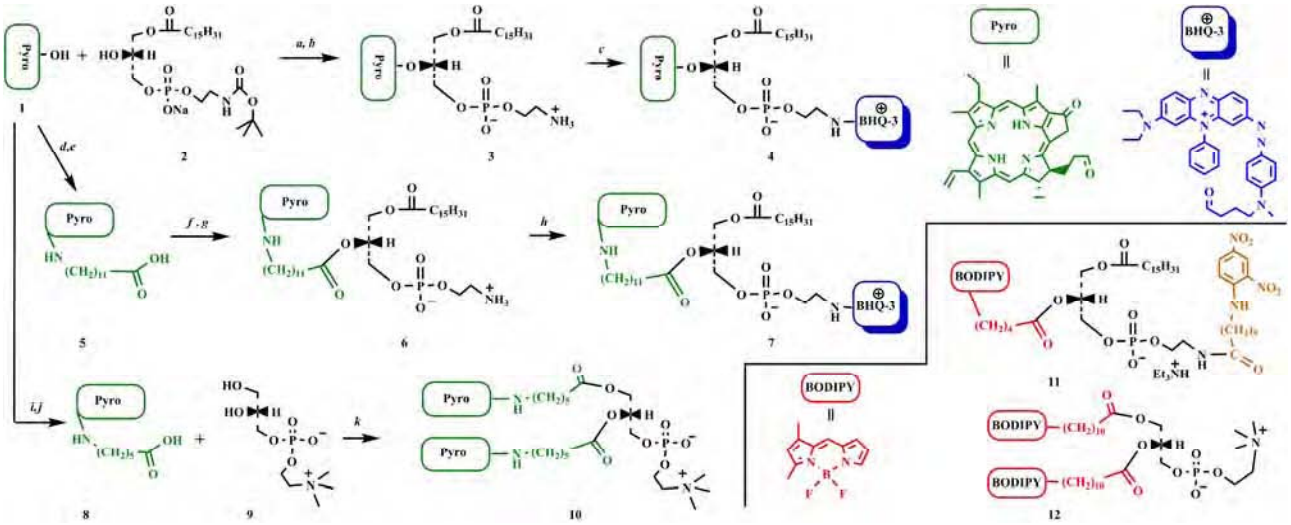

Reagents, conditions (all reactions were performed under Ar in dark) and isolated yields (relative to starting NIRF **1**, one arrow indicates one-pot reaction): (a) EDC, DMAP, DCM, rt, 72 h; (b) TFA, DCM, 0 °C, 4 h, 20%; (c) BHQ-3$^+$-SU PF_6^-, TEA, DCM, rt 12 h, 15%; (d) NHS, EDC, DMAP, DCM, rt, 3 h; (e) $H_2N(CH_2)_{11}CO_2H$, TEA, DCM, rt, 72 h, 85% (f) **2,** EDC, DMAP, DCM, rt, 72 h; (g) TFA, DCM, 0 °C, 4 h, 15%; (h) BHQ-3$^+$-SU PF_6^-, TEA, DCM, rt 12 h, 10%; (i) NHS, EDC, DMAP, DCM, rt, 3 h; (j) $H_2N(CH_2)_5CO_2H$, TEA, DCM, rt, 72 h, 75%; (k) EDC, DMAP, DCM, 40 °C, 85 h, 8%

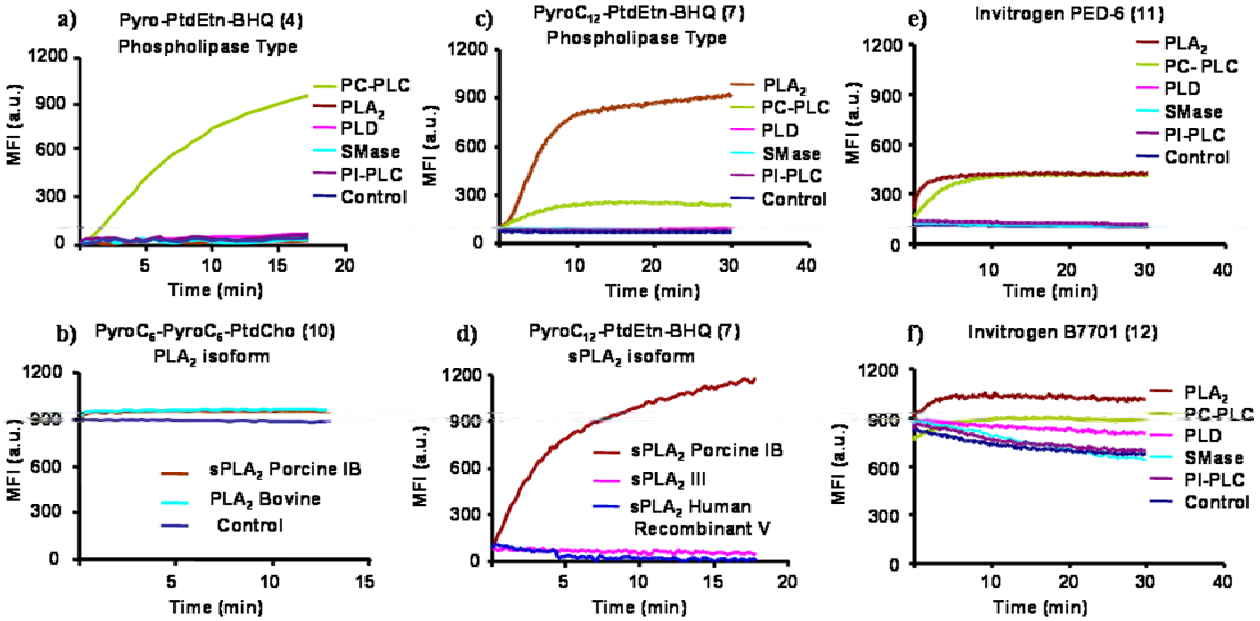

Figure 3. Sensitivity of self-quenched fluorescent probes to different phospholipase isoforms as measured by fluorescence release on a plate reader.

Scheme 1 demonstrates the synthesis of three self-quenched Pyro-bearing probes **4**, **7** and **10**. NIRF acid **1** was coupled with *N*-BOC *Lyso*-phosphatidylethanolamine (*Lyso*-PtdEtn, **2**) under basic conditions in order to conserve the steric configuration at the *sn*-2 site and avoid racemization.[6] Next TFA-mediated BOC-deprotection resulted in the permanently fluorescent Pyro-PtdEtn (**3**). In the final step BHQ-3 was attached to the amino group of lipid **3** resulting in a self-quenching Pyro-PtdEtn-BHQ (**4**). To incorporate spacers we have synthesized $PyroC_{12}$- (**5**) and $PyroC_6$- (**8**) acids. Acid **5** was used as described above with acid **1** for production of the permanent lipid fluorophore $PyroC_{12}$-PtdEtn (**6**), which was then converted into its self-quenched derivative (**7**). Two molecules of acid **8** were conjugated with *sn*-glycero-3-phosphocholine (**9**) to give rise to $PyroC_6$-$PyroC_6$-PtdCho (**10**) where self-quenching is achieved by interactions between the two NIRFs.

Farber *et al.* had demonstrated that PLA_2 activity can be detected by visual fluorescence in transparent zebra fish larvae.[7] These and other probes are now available commercially (Scheme 1, compounds **11**, **12**). The sensitivity of those phospholipids **11**, **12** to PLs other than PLA_2 was not tested at that time. As seen from Scheme 1 compounds **4**, **7** and **11** have a fluorophore attached at the *sn*-2 position and a quencher bound to the nitrogen atom of the PE head. Compounds **10** and **12** exploit self-quenching of two of the same fluorophores attached to the *sn*-1 and *sn*-2 positions.

We have tested our three self-quenched probes **4**, **7** and **10** as well as commercial probes **11** and **12** as substrates for different phospholipases. The results are presented in Figure 3. Probe **4** revealed high selective sensitivity to PLC, particularly to the PC-PLC isoform (Fig. 3a), while sensitivity to other tested phospholipases including PLA_2 is negligible. NIRF compounds **10** and **7** were tested as potential PLA_2-sensitive probes in comparison with their visible counterparts **12** and **11**, respectively. PtdCho **10** revealed significant background fluorescence (Fig. 3b) because both substituents at *sn*-1 and *sn*-2 positions are self-fluorescent and their quenching efficiency is not high. Only a modest (10%) fluorescence increase was detected under the action of PLA_2, similar to those observed for the visible analog **12** (Fig. 3f). In contrast the C_{12}-spacered PtdEtn **7** demonstrated a remarkable selectivity for PLA_2 (Fig. 3c) and the best relative PLA_2/PLC sensitivity, significantly outperforming the magnitude of the best previously known probe **11** (Fig. 3e). Moreover, this construct exhibited significant PLA_2 isoform specificity with Porcine sPLA$_2$ IB demonstrating the highest activity (Fig. 3d).

In conclusion, we have designed, synthesized and tested for the first time near-infrared self-quenched phospholipid probes that reveal high sensitivity to PLC and PLA_2. These results open an avenue for future *in vivo* experiments with mammals and for the development of sensitive new probes to detect PL activity.

Acknowledgment. Financial support was provided by the NIH (grants R01CA114347 and R01CA129176 (EJD)), DoD (W81XWH-08-1-0716 (AVP)) and Bracco Research USA.

Supporting Information Available: Experimental procedures and characterization. This material is available free of charge via the Internet at http://pubs.acs.org.

References

(1) (a) Cevc, G.; Editor *Phospholipids Handbook*, 1993. (b) Hanahan, D. J. *A Guide to Phospholipid Chemistry*, 1997. (c) Wilton, D. C. *Biochem. Lipids, Lipoproteins Membr. (5th Ed.)* **2008**, 305-329.

(2) (a) Sved, P.; Scott, K. F.; McLeod, D.; King, N. J. C.; Singh, J.; Tsatralis, T.; Nikolov, B.; Boulas, J.; Nallan, L.; Gelb, M. H.; Sajinovic, M.; Graham, G. G.; Russell, P. J.; Dong, Q. *Cancer Res.* **2004**, *64*, 6934-6940. (b) Yamashita, S.-i.; Ogawa, M.; Sakamoto, K.; Abe, T.; Arakawa, H.; Yamashita, J.-i. *Clin. Chim. Acta* **1994**, *228*, 91-99. (c) Stefanski, E.; Pruzanski, W.; Sternby, B.; Vadas, P. J. *Biochem.* **1986**, *100*, 1297-1303.

(3) (a) Degani, H.; DeJordy, J. O.; Salomon, Y. *Proc. Natl. Acad. Sci. U. S. A.* **1991**, *88*, 1506-1510. (b) Spadaro, F.; Ramoni, C.; Mezzanzanica, D.; Miotti, S.; Alberti, P.; Cecchetti, S.; Iorio, E.; Dolo, V.; Canevari, S.; Podo, F. *Cancer Res.* **2008**, *68*, 6541-6549. (c) Soderquist, A. M.; Todderud, G.; Carpenter, G. *Cancer Res.* **1992**, *52*, 4526-4529. (d) Bertagnolo, V.; Benedusi, M.; Brugnoli, F.; Lanuti, P.; Marchisio, M.; Querzoli, P.; Capitani, S. *Carcinogenesis* **2007**, *28*, 1638-1645.

(4) (a) Ntziachristos, V.; Bremer, C.; Weissleder, R. *Eur. Radiol.* **2003**, *13*, 195-208. (b) Mahmood, U.; Weissleder, R. *Mol. Cancer Ther.* **2003**, *2*, 489-496.

(5) (a) Lo, P.-C.; Chen, J.; Stefflova, K.; Warren, M. S.; Navab, R.; Bandarchi, B.; Mullins, S.; Tsao, M.; Cheng, J. D.; Zheng, G. *J. Med. Chem.* **2009**, *52*, 358-368. (b) Stefflova, K.; Chen, J.; Marotta, D.; Li, H.; Zheng, G. *J. Med. Chem.* **2006**, *49*, 3850-3856.

(6) (a) Lindberg, J.; Ekeroth, J.; Konradsson, P. J. *Org. Chem.* **2002**, *67*, 194-199. (b) Rosseto, R.; Bibak, N.; DeOcampo, R.; Shah, T.; Gabrielian, A.; Hajdu, J. *J. Org. Chem.* **2007**, *72*, 1691-1698.

(7) (a) Farber, S. A.; Pack, M.; Ho, S.-Y.; Johnson, L. D.; Wagner, D. S.; Dosch, R.; Mullins, M. C.; Hendrickson, H. S.; Hendrickson, E. K.; Halpern, M. E. *Science* **2001**, *292*, 1385-1388. (b) Hendrickson, H. S.; Hendrickson, E. K.; Johnson, I. D.; Farber, S. A. *Anal. Biochem.* **1999**, *276*, 27-35.

Table of Content Graphic

Design and Synthesis of Phospholipase C and A_2-Activatable Near Infrared Fluorescent Smart Probes

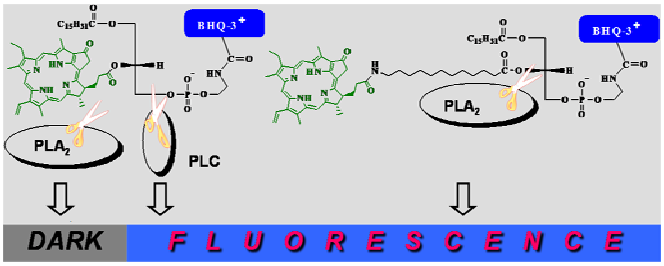

Abstract

The primary focus of this work was to develop activatable probes suitable for *in vivo* detection of phospholipase activity. Phospholipases (PLs) are ubiquitous enzymes that perform a number of critical regulatory functions. They catalyze phospholipid breakdown and are categorized as A_1, A_2 (PLA_2), C (PLC) and D (PLD) based on their site of action. Here we report the design, synthesis and characterization of self-quenching reporter probes that release fluorescent moieties upon cleavage with PLA_2 or PLC. A series of phospholipids were synthesized bearing the NIR fluorophore Pyropheophorbide *a* (Pyro) at the *sn*2-position. Fluorescence quenching was achieved by attachment of either a positively charged Black Hole Quencher-3 (BHQ-3) to the phospholipid head group or another neutral Pyro moiety at the *sn*1-position. The specificity to different phospholipases was modulated by insertion of spacers (C_6, C_{12}) between Pyro and the lipid backbone. The specificity of the quenched fluorescent phospholipids were assayed on a plate reader against a number of phospholipases and compared with two commercial probes bearing the visible fluorophore BODIPY. While PyroC_6-PyroC_6-PtdCho revealed significant background fluorescence, and a10% fluorescence increase under the action of PLA_2, Pyro-PtdEtn-BHQ demonstrated high selective sensitivity to PLC, particularly to the PC-PLC isoform, and its sensitivity to PLA_2 was negligible due to steric hindrance at the *sn*2-position. In contrast, the C_{12}-spacered PyroC_{12}-PtdEtn-BHQ demonstrated a remarkable selectivity for PLA_2 and the best relative PLA_2/PLC sensitivity, significantly outperforming previously known probes. These results open an avenue for future *in vivo* experiments and for new probes to detect PL activity.

Supporting Information

Design and Synthesis of Phospholipase C and A_2-Activatable Near Infrared Fluorescent Smart Probes

Anatoliy V. Popov,*[,†] Theresa M. Mawn,[†] Soungkyoo Kim,[†] Gang Zheng,[†,‡] and E. James Delikatny[†]

[†]*University of Pennsylvania, Department of Radiology, Philadelphia PA, 19104, USA*

[‡]*University of Toronto, Department of Medical Biophysics, Toronto ON, M5G 1L7, Canada*

E-mail: avpopov@mail.med.upenn.edu

Table of Contents

List of abbreviations

BHQ-3 carboxylic acid – black hole quencher-3, 3-diethylamino-5-phenylphenazium-7-diazobenzene-4"-(*N*-methyl)-*N*-butyric acid

BHQ-3^{+}-SU PF_6^{-} – succinimidyl ester of BHQ-3 carboxylic acid, hexafluorophosphate

BOC – *tert*-butoxycarbonyl

Cho – choline

DCM – dichloromethane, CH_2Cl_2

DMAP – 4-dimethylaminopyridine

EDC – 1-ethyl-3-(3-dimethylaminopropyl) carbodiimide, hydrochloride salt

Etn – ethanolamine

$H_2N(CH_2)_{11}CO_2H$ – λ-aminolauric acid

$H_2N(CH_2)_5CO_2H$ – ε-aminocaproic acid

Invitrogen PED6 – *N*-((6-(2,4-dinitrophenyl)amino)hexanoyl)-2-(4,4-difluoro-5,7-dimethyl-4-bora-3a,4a-diaza-*s*-indacene-3-pentanoyl)-1-hexadecanoyl-*sn*-glycero-3-phosphoethanolamine, triethylammonium salt

Invitrogen B77101 – 1,2-bis-(4,4-difluoro-5,7-dimethyl-4-bora-3a,4a-diaza-*s*-indacene-3-undecanoyl)-*sn*-glycero-3-phosphocholine

MALDI-TOF – Matrix Assisted Laser Desorption/Ionization Time-of-Flight Mass Spectrometry

N-BOC *Lyso* PtdEtn – 1-palmytoyl-*sn*-glycero-3-phosphoethanolamine-*N*-(*tert*-butoxycarbonyl) (sodium salt)

NHS – *N*-hydroxysuccinimide

NIR – near infrared

NIRF – near infrared fluorophore

PC – phosphocholine

PC-PLC – phosphatidylcholine-specific phospholipase C

PC-PLD – phosphatidylcholine-specific phospholipase D

PE – phosphoethanolamine

PI-PLC – phosphatidylinositol-specific phospholipase C

PL – phospholipase

PLs – phospholipases

PtdCho – phosphatidylcholine

PtdEtn – phosphatidylethanolamine

Pyro – pyropheophorbide *a*

Pyro-SU – succinimidyl ester of pyropheophorbide *a*

PyroC_{12} acid – λ-Pyropheophorbideamidolauric acid or 17^3-deoxy-17^3-(α-carbhydroxyundecylene-λ- amino)pyropheophorbide *a*

PyroC_{12}-PtdEtn – 1-palmitoyl-2-(λ-pyropheophorbideamidolauroyl)-*sn*-glycero-3-phosphoethanolamine

PyroC_{12}-PtdEtn-BHQ – 1-palmitoyl-2-(λ-pyropheophorbideamidolauroyl)-*sn*-glycero-3-phosphoethanolamide of BHQ-3 carboxylic acid

PyroC_6 acid – ε-Pyropheophorbideamidocaproic acid or 17^3-deoxy-17^3-(α-carbhydroxypentylene-ε-amino)pyropheophorbide *a*

PyroC_6-PyroC_6-PtdCho – 1,2-bis(ε-pyropheophorbideamidocaproyl)-*sn*-glycero-3-phosphocholine

Pyro-PtdEtn – 1-palmitoyl-2-pyropheophorbide-*sn*-glycero-3-phosphoethanolamine

Pyro-PtdEtn-BHQ – 1-palmitoyl-2-pyropheophorbide-*sn*-glycero-3-phosphoethanolamide of BHQ-3 carboxylic acid

SMase – sphingomyelinase

sPLA_2 – secretory phospholipase A_2

TEA, Et_3N – triethylamine

TFA – trifluoroacetic acid

TLC – thin layer chromatography

I. General Information

Dry solvents were purchased from ACROS Organics. Regular solvents and Celite were purchased from Fisher Scientific. *Spirulina Pacifica* algae (the starting material for Pyropheophorbide *a*) was purchased from Cyanotech Corporation, Kailua-Kona, HI, USA. *N*-BOC *Lyso* PtdEtn (N-Boc16:0 Lyso PE) was purchased from Avanti Polar Lipids, Inc., Alabaster, AL, USA. BHQ-3 carboxylic acid succinimidyl ester hexafluorophosphate was purchased from Bioresearch Technologies, Novato, CA, USA. Other reagents/reactants were purchased from Sigma-Aldrich and used without further purification. Silica Gel Standard Grade

(230x450 mesh) was purchased from Sorbent Technologies, Atlanta, GA, USA. Thin Layer Chromatography Plates, Partsil® PK6F, Silica Gel 60 Å, 20x20 cm, were purchased from Whatman, washed with EtAc-MeOH (60:40, v/v) and baked at 150 °C overnight before use. All chemical reactions with pyropheophorbide *a* and its derivatives were carried out in the dark under dry Ar. ^{1}H NMR spectra were recorded using a Bruker DMX 360 MHz spectrometer. MALDI-TOF mass-spectra were recorded with an Applied Biosystems Voyager DE Mass Spectrometer using a positive mode ionization and CHCA (α-Cyano-4-hydroxycinnamic Acid) or HABA (2-(4-hydroxyphenylazo)benzoic acid) matrix. Time-dependent release of fluorescence was measured using a SpectraMax M5 fluorescent plate reader.

PC-PLC (*Bacillus cereus*), PI-PLC (*B. cereus*), SMase (*B. cereus*), PC-PLD (*Streptomyces chromofuscus*), type IA sPLA$_2$ (*naja mossambica mossambica*), type IB sPLA$_2$ (porcine pancreas), and type IB sPLA$_2$ (bovine pancreas) were obtained from Sigma (St. Louis, MO). Human recombinant type V sPLA2 was obtained from ProSpec-Tany TechnoGene, Ltd. (Rehovot, Israel). Phospholipases were dissolved in Tris buffer (50 mM Tris-HCl, pH 7.4) and stored in aliquots at -20 °C.

II. Synthesis

Pyropheophorbide *a* (**1**) was prepared from *Spirulina Pacifica* algae according to procedure [1].

General procedure for synthesis of *N*-Pyropheophorbide substituted ω-amino acids (PyroC$_6$ and PyroC$_{12}$ acids)

A 200 mL round bottom flask was charged with pyropheophorbide acid (**1**) (0.38 mmol), NHS (0.38 mmol), EDC (0.38 mmol), DMAP (23.3 mg. 0.19 mmol) and 200 ml of dry DCM. The reaction mixture was stirred in dark under Ar for 3 h until Pyropheophorbide acid was converted completely into its succinimidyl ester (TLC $CHCl_3$/MeOH = 5/1, v/v). Then $H_2N(CH_2)_nCO_2H$ (n = 5, 11, 0.38 mmol) and dry pyridine (25 ml) were added. The second reaction was carried out for 48 h until complete conversion of Pyro-SU. The solvents were then evaporated; the solid residue was dissolved in 100 ml of GCM, rinsed twice with 2% HCl, then water. The product

was isolated by column chromatography on silica gel using (DCM-ethyl acetate (0-100%), then ethyl acetate-MeOH (0-40%)). Isolated yields are 75-85%.

ε-Pyropheophorbideamidocaproic acid or 17^3-deoxy-17^3-(α-carbhydroxypentylene-ε-amino)pyropheophorbide *a*, PyroC_6 acid (8)

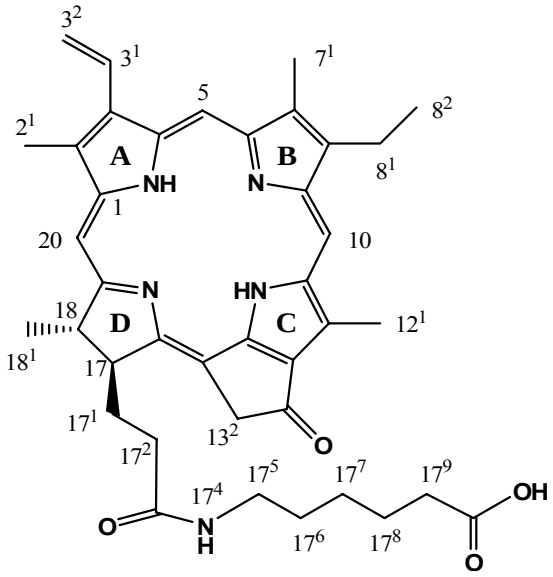

Yield 75%. ^{1}H NMR (360 MHz, $CDCl_3$, CD_3OD δ ppm): 9.14, 9.02 and 8.38 (each s, 1H, 5-*H*, 10-*H* and 20-*H*); 7.74 (dd, J=11.5 Hz, J=17.6 Hz, 1H, 3^1-C*H*=CH_2); 6.09 (d, J=17.6 Hz, 1H, *trans*-3^2-CH=CH*H*); 5.99 (d, J=11.5 Hz, 1H, *cis*-3^2-CH=C*H*H); 5.03 (AB, A=5.11, B=4.96, J_{AB}=20.2 Hz, 2H, 13^2-CH_2); 4.32 (q, J=8.1 Hz, 1H, 18-*H*); 4.12 (dm, 8.7 Hz, 1H, 17-*H*); 3.45-3.32 m 5H, 3.27-3.12 m 5H and 2.94 s 3H (2 ^{1}-CH_3, 12^1-CH_3, 7^1-CH_3, 8^1-CH_2, 17^5-CH_2); 2.61-2.39 m 2H and 2.31-2.08 m 4H (17^2-CH_2, 17^9-CH_2, 17^1-CH_2); 1.77-1.40 m 10H (18^1-CH_3, 8^2-CH_3, 17^6-CH_2, 17^8-CH_2); 1-36-1.21 (m, 2H, 17^7-CH_2). MALDI-TOF, *m/z*: $(M+Na)^+$ 670.41, calculated for $C_{39}H_{45}N_5NaO_4$ 670.34.

λ-Pyropheophorbideamidolauric acid or 17^3-deoxy-17^3-(α-carbhydroxyundecylene-λ-amino)pyropheophorbide *a*, PyroC_{12} acid (5)

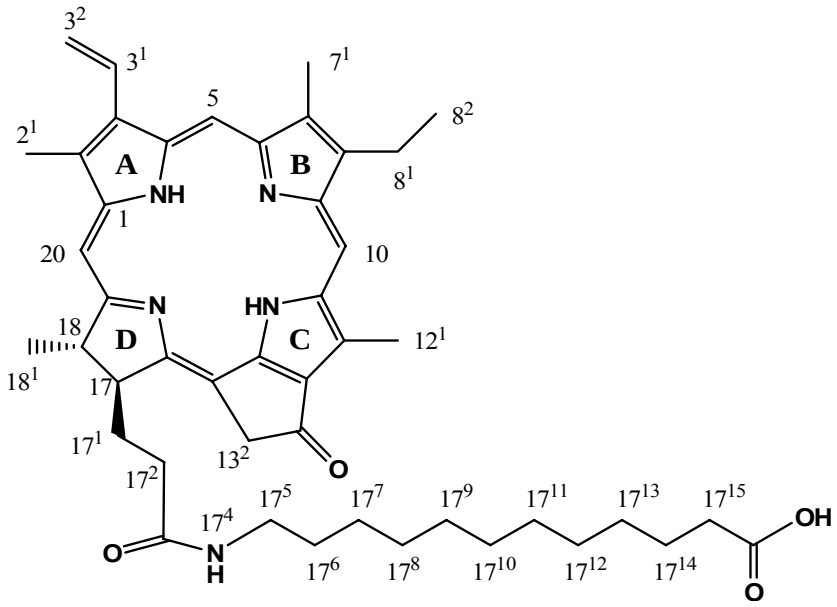

Yield 85%. ^{1}H NMR (360 MHz, $CDCl_3$, CD_3OD δ ppm): 9.17, 9.06 and 8.41 (each s, 1H, 5-*H*, 10-*H* and 20- *H*); 7.77 (dd, J=11.5 Hz, J=17.6 Hz, 1H, 3^{1}-C*H*=CH_2); 6.11 (d, J=17.6 Hz, 1H, *trans*-3^{2}-CH=CH*H*); 6.02 (d, J=11.5 Hz, 1H, *cis*-3^{2}-CH=C*H*H); 5.06 (AB, A=5.14, B=4.99, J_{AB}=20.2 Hz, 2H, 13^{2}-CH_2); 4.36 (q, J=8.1 Hz, 1H, 18- *H*); 4.15 (dm, 8.7 Hz, 1H, 17- *H*); 3.51-3.35 m 5H, 3.30-3.14 m 5H and 2.98 s 3H (2^{1}-CH_3, 12^{1}-CH_3, 7^{1}-CH_3, 8^{1}-CH_2, 17^{5}-CH_2); 2.67-2.41 m 2H and 2.35-2.08 m 4H (17^{2}-CH_2, 17^{15}-CH_2, 17^{1}-CH_2); 1.79-1.46 m 10H (18^{1}-CH_3, 8^{2}-CH_3, 17^{6}-CH_2, 17^{14}-CH_2); 1.44-1.12 (m, 14H, 17^{7}-17^{13} 7xCH_2). MALDI-TOF, *m/z*: $(M+Na)^+$ 754.51, calculated for $C_{45}H_{57}N_5NaO_4$ 754.43.

General procedure for synthesis of 2-pyropheophorbide *a* (with and without C_{12} spacer) substituted 1-palmitoyl-*sn*-glycero-3-phosphoethanolamines

A 200 mL dry flask was charged with *N*-BOC *Lyso* PtdEtn (0.87 mmol), a Pyro-containing acid (0.87 mmol), EDC (1.30 mmol), DMAP (0.43 mmol) and DCM (70 mL). The conversion of Pyro-acid was monitored by TLC ($CHCl_3$/MeOH = 4/2). After 72 h the reaction mixture was diluted with hexanes (30 mL) and passed through a small column with Celite to eliminate non-soluble by-products. After evaporation of solvents, the solid was dissolved in a small amount of DCM and moved into a dry 100 mL flask. After solvent evaporation the residue was dried under high vacuum overnight. Then dry DCM (25 mL) was added, the flask was cooled until -20 °C and TFA (5 mL) was added. The BOC-deprotection reaction was carried out at 0 °C 4 h. Following that, dry toluene (20 mL) was added (to avoid TFA concentrating under evaporation)

and volatiles were removed under vacuum . The so lid residue was treated with 5% solution of Et_3N in DCM (30 m L) to neutralize traces of TF A. After liquids evaporation the residue was dried under high vacuum overnight. This residue was then dissolved in dry $CHCl_3$ and put onto 6 preparative TLC plates. Preparative TLC (20% MeOH in $CHCl_3$) resulted in th e Pyro-PtdEtn derivative as a dark green amorphous solid.

1-palmitoyl-2-pyropheophorbide-*sn*-glycero-3-phosphoethanolamine, Pyro-PtdEtn (3)

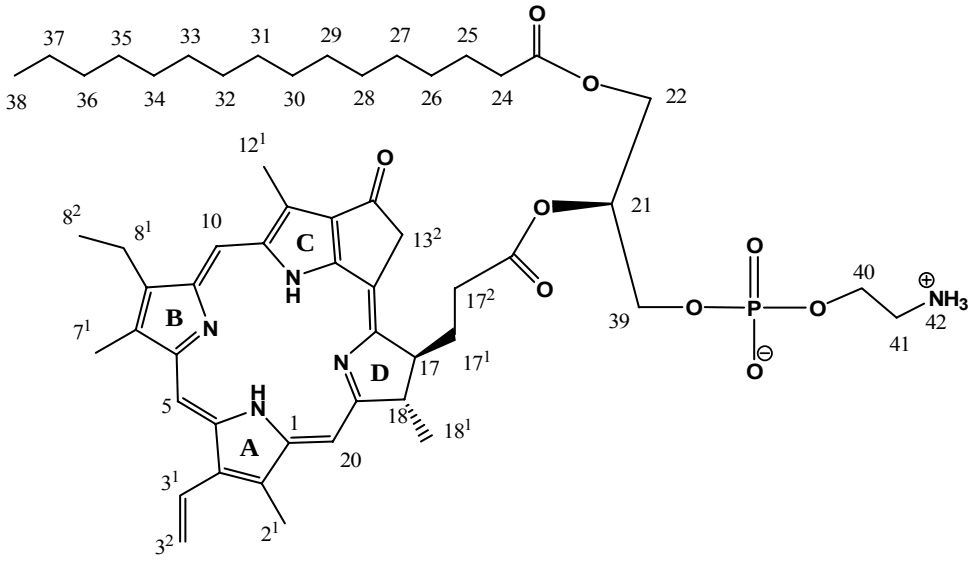

Yield 20%. R_f = 0.40 ($CHCl_3/CH_3OH$ = 4/1, v/v). ^{1}H NMR (360 MHz, $CDCl_3/CD_3OD$, δ ppm): 9.37, 9.28 and 8.50 (each s, 1H, 5- *H*, 10-*H* and 20-*H*); 7.93 (dd, J=11.5 Hz, J=17.6 Hz, 1H, 3^1-C*H*=CH_2); 6.24 (d, J=17.6 Hz, 1H, *trans*-3^2-CH=CH*H*); 6.13 (d, J=11.5 Hz, 1H, *cis*-3^2-CH=C*H*H); 5.40-5.01 m 3H (21-*H*, 13^2-CH_2); 4.45 m 2H and 4.32-3.94 m 6H (18-H, 17-H, 22-CH_2, 39-CH_2, 40-CH_2); 3.71-3.51 m 5H, 3.47-3.29 m 5H and 3.18 s 3H (2^1-CH_3, 12^1-CH_3, 7^1-CH_3, 8^1-CH_2, 41-CH_2); 3.12-2.53 m 2H and 2.41-2.14 m 4H (17^2-CH_2, 24-CH_2, 17^1-CH_2); 1.85-1.56 m 8H and 1.45-1.14 m 24H (18^1-CH_3, 8^2-CH_3, 25-37 13xCH_2); 1.05-0.87 (m, 3H, 38-CH_3). MALDI-TOF, *m/z*: $(M+Na)^+$ 992.69, calculated for $C_{54}H_{76}N_5NaO_9P$ 992.53.

1-palmitoyl-2-(λ-pyropheophorbideamidolauroyl)-*sn*-glycero-3-phosphoethanolamine, PyroC$_{12}$-PtdEtn (6)

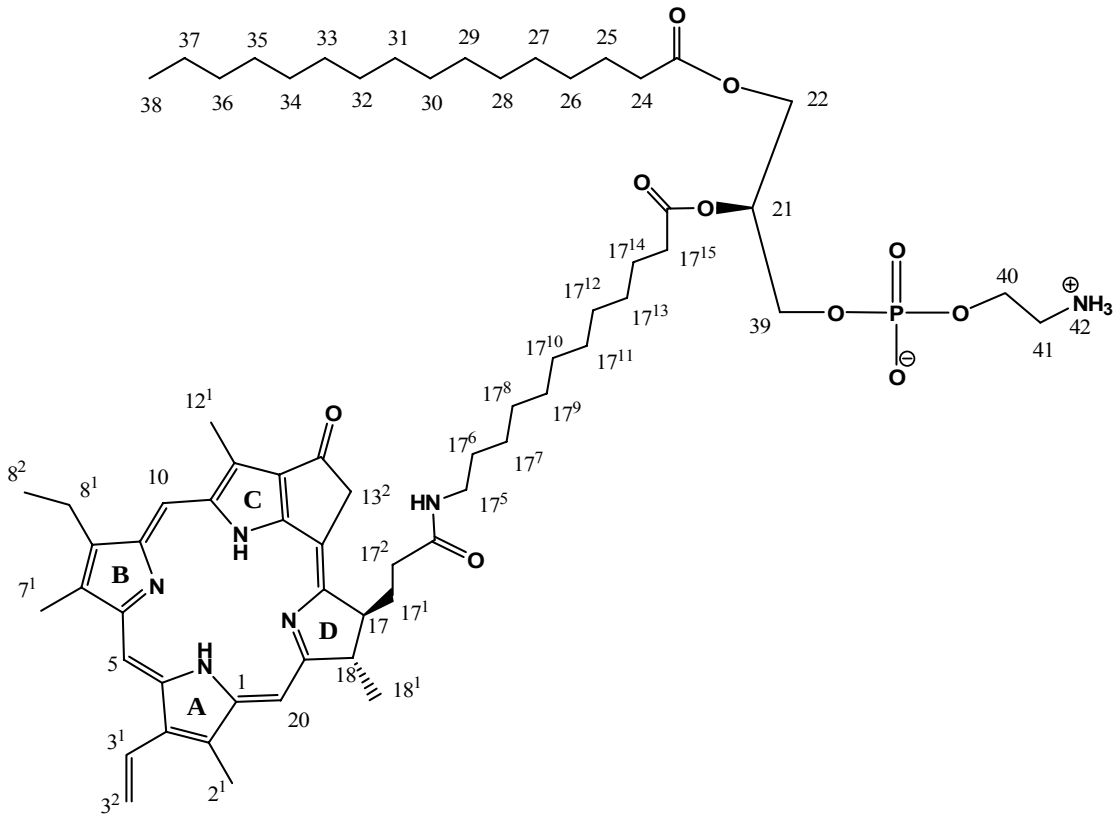

Yield 18%. R_f = 0.25 ($CHCl_3/CH_3OH$ = 4/1, v/v). ^{1}H NMR (360 MHz, $CDCl_3/CD_3OD$, CD_2Cl_2, δ ppm): 9.18, 9.07 and 8.42 (each s, 1H, 5-*H*, 10-*H* and 20-*H*); 7.79 (dd, J=11.5 Hz, J=17.6 Hz, 1H, 3^1-C*H*=CH_2); 6.13 (d, J=17.6 Hz, 1H, *trans*-3^2-CH=CH*H*); 6.04 (d, J=11.5 Hz, 1H, *cis*-3^2-CH=C*H*H); 5.18-4.93 m 3H (21-*H*, 13^2-CH_2, overlapped partially with CD_2Cl_2); 4.60-3.96 m 8H (18-*H*, 17-*H*, 22-CH_2, 39-CH_2, 40-CH_2); 3.55-2.91 m, m and s 15H, (2^1-CH_3, 12^1-CH_3, 7^1-CH_3, 8^1-CH_2, 17^5-CH_2, 41-CH_2); 2.64-2.11 m 8H (17^2-CH_2, 24-CH_2, 17^1-CH_2, 17^{15}-CH_2); 1.85-1.14 m 50H (18^1-CH_3, 8^2-CH_3, 25-37 and 17^6-17^{14} 22xCH_2); 1.06-0.90 (m, 3H, 38-CH_3). MALDI-TOF, *m/z*: $(M+Na)^+$ 1189.86, calculated for $C_{66}H_{99}N_6NaO_{10}P$ 1189.71.

General procedure for synthesis of Pyro-PtdEtn-BHQ and PyroC_{12}-PtdEtn-BHQ

A 100 mL flask was loaded with a Pyro-containing PtdEtn (**3** or **6**) (0.013 mmol), BHQ-3^+-SU PF_6^- (0.013 mmol) and 50 mL of dry DCM. After dissolution 1 drop of Et_3N was added. The reaction was carried out for 4 h. Volatiles were removed in a rotary evaporator and the residue was dried under high vacuum overnight. The residue was dissolved in $CHCl_3$ and put onto 4

preparative TLC plates. Thin layer preparative chromatography gave in result the final product as a dark sea-green amorphous solid.

1-palmitoyl-2-pyropheophorbide-*sn*-glycero-3-phosphoethanolamide of BHQ-3 carboxylic acid, Pyro-PtdEtn-BHQ (4)

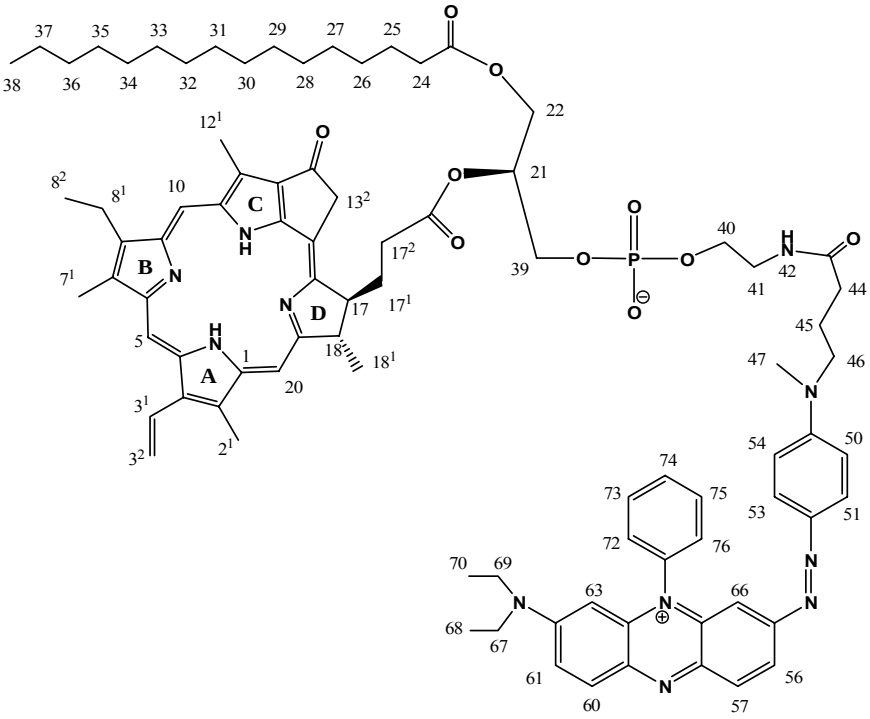

Yield 75%. R_f = 0.6 ($CHCl_3/CH_3OH$ = 5/1, v/v). ^{1}H NMR (360 MHz, $CDCl_3$, CD_3OD, δ ppm): 9.39, 9.29 and 8.54 (each s, 1H, 5- *H*, 10-*H* and 20-*H*); 8.09-6.46 m 16H (50-*H*, 51-*H*, 53-*H*, 54-*H*, 56-*H*, 57-*H*, 60-*H*, 61-*H*, 63-*H*, 72-76 5x *H*, 3^1-C*H*=CH_2, overlapped partially with $CDCl_3$); 6.26 (d, J=17.6 Hz, 1H, *trans*-3^2-CH=CH*H*); 6.15 (d, J=11.5 Hz, 1H, *cis*-3^2-CH=C*H*H); 5.33-5.05 m 3H (21- *H*, 13^2-CH_2); 4.51-3.89 (m , 8H, 18- *H*, 17-*H*, 22-CH_2, 39-CH_2, 40-CH_2); 3.70-3.08 m 19H and 2.90 s 3H (2^1-CH_3, 12^1-CH_3, 7^1-CH_3, 47-CH_3 8^1-CH_2, 41-CH_2, 46-CH_2, 67-CH_2, 69-CH_2); 2.74-2.14 (m , 8H, 17^2-CH_2, 24-CH_2, 17^1-CH_2, 44-CH_2); 1.96-1.10 (m , 40H, 18^1-CH_3, 8^2-CH_3, 68-CH_3, 70-CH_3, 25-37 and 46- 14xC H_2); 1.04-0.86 (m , 3H, 38-C H_3). MALDI-TOF, *m/z*: $(M+Na)^+$ 1520.93, calculated for $C_{87}H_{108}N_{11}NaO_{10}P$ 1520.79.

1-palmitoyl-2-(λ-pyropheophorbideamidolauroyl)-*sn*-glycero-3-phosphoethanolamide of BHQ-3 carboxylic acid, PyroC_{12}-PtdEtn-BHQ (7)

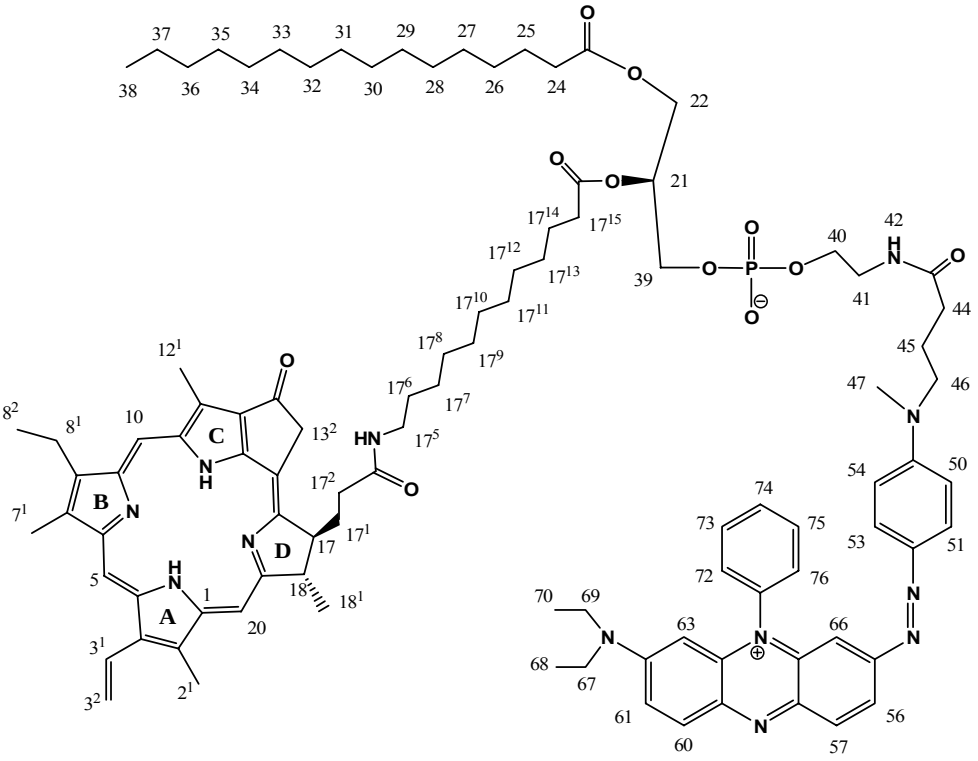

Yield 57%. R_f = 0.3 ($CHCl_3/CH_3OH$ = 5/1, v/v). ^{1}H NMR (360 MHz, $CDCl_3$,CD_3OD, CD_2Cl_2, δ ppm): 9.19, 9.09 and 8.44 (each s, 1H, 5- *H*, 10-*H* and 20-*H*); 8.06-6.52 m 16H (50-*H*, 51-*H*, 53-*H*, 54- *H*, 56- *H*, 57- *H*, 60- *H*, 61- *H*, 63- *H*, 72-76 5x *H*, 3 ^{1}-C*H*=CH_2, overlapped partially with $CDCl_3$); 6.14 (d, J=17.6 Hz, 1H, *trans*-3^2-CH=CH*H*); 6.05 (d, J=11.5 Hz, 1H, *cis*-3^2-CH=C*H*H); 5.24-4.93 m 3H (21-*H*, 13^2-CH_2, overlapped partially with CD_2Cl_2); 4.65-3.94 (m, 8H, 18-*H*, 17-*H*, 22-CH_2, 39-CH_2, 40-CH_2); 3.59-3.13 m 18H, 2.98 s 3H and 2.90 s 3H (2 ^{1}-CH_3, 12^1-CH_3, 7^1-CH_3, 47-CH_3, 8 ^{1}-CH_2, 17 ^{5}-CH_2, 41-CH_2, 46-CH_2, 67-CH_2, 69-CH_2); 2.64-2.10 (m , 10H, 17 ^{2}-CH_2, 24-CH_2, 17^1-CH_2, 17^{15}-CH_2, 44-CH_2); 1.93-1.08 (m , 58H, 18 ^{1}-CH_3, 8^2-CH_3, 68-CH_3, 70-CH_3, 25-37, 46- and 17^6-17^{14} 23xCH_2); 1.05-0.95 (m, 3H, 38-CH_3). MALDI-TOF, *m/z*: $(M+Na)^+$ 1718.14, calculated for $C_{99}H_{131}N_{12}NaO_{11}P$ 1717.97.

Synthesis of 1,2-bis(ε-pyropheophorbideamidocaproyl)-*sn*-glycero-3-phosphocholine, PyroC$_6$-PyroC$_6$-PtdCho (10)

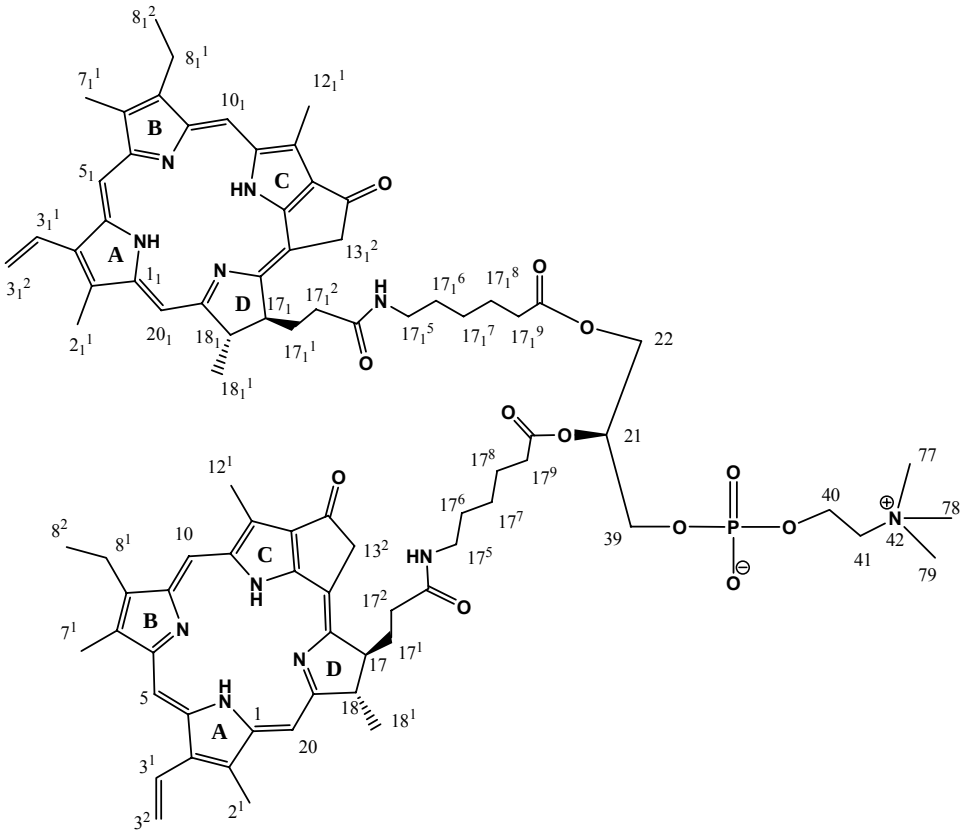

A 100 mL flask was loaded with *sn*-glycero-3-phosphocholine (**9**) (0.026 mmol), ε-Pyropheophorbideamidocaproic acid (**8**) (0.077 mmol), and 50 mL dry MeOH. The mixture was stirred 1h at rt. Then methanol was evaporated under low pressure and the resulting film was dried under high vacuum overnight. Next, EDC (0.077 mmol), DMAP (0.077 mmol) and dry DCM (50 mL) were added to the flask. The reaction mixture was stirred in dark under Ar at 40 °C for 85 h. After that the solution was rinsed with 0.5N HCl, and dried over Na_2SO_4. After solvent evaporation the mixture was dissolved in DCM and put onto three preparative TLC plates. Preparative TLC with $CHCl_3$/MeOH (3/1, v/v) resulted in a mixture of mono- and disubstituted *sn*-glycero-3-phosphocholines (R_f=0.1-0.2). The latter was separated a second time on TLC plates with $CHCl_3$/MeOH/H_2O (2/1/1, v/v/v). The target product (R_f=0.35, $CHCl_3$/MeOH/H_2O = 2/1/1, v/v/v) was isolated with the yield of 11% as an amorphous dark green solid. ^{1}H NMR (360 MHz, CDCl$_3$, CD_3OD, CD_2Cl_2, δ ppm): 9.36, 9.27, 9.16, 9.04, 8.49, and 8.40 (each s, 1H, 5-*H*, 10-*H*, 20-*H*, 5_1-*H*, 10_1-*H* and 20_1-*H*); 7.99-7.70 (m, 2H, 3^1-*H* and $3_1{}^1$-*H*), 6.30-5.98 (m, 4H, 3^2-CH_2 and $3_1{}^2$-CH_2), 5.33-4.93 (m, 5H, 21-*H*, 13^2-CH_2 and $13_1{}^2$-CH_2, overlapped partially with CD_2Cl_2); 4.52-3.90 (m, 10H, 18-*H*, 17-*H*, 18_1-*H*, 17_1-*H*, 22-CH_2, 39-CH_2, 40-CH_2); 3.67-2.93 (m, 37H, 2^1-CH_3, $2_1{}^1$-CH_3, 12^1-CH_3, $12_1{}^1$-CH_3, 7^1-CH_3, $7_1{}^1$-CH_3, 77-

C*H*$_3$, 78-C*H*$_3$, 79-C*H*$_3$, 8^1-C*H*$_2$, 8$_1$^{1}-C*H*$_2$, 17^5-C*H*$_2$, 17$_1$^{5}-C*H*$_2$, 41-C*H*$_2$, overlapped partially with CD_3OD); 2.71-2.10 (m, 12H, 17^2-C*H*$_2$, 17^9-C*H*$_2$, 17^1-C*H*$_2$, 17$_1$^{2}-C*H*$_2$, 17$_1$^{9}-C*H*$_2$, 17$_1$^{1}-C*H*$_2$); 1.83-1.46 (m, 20H, 18 ^{1}-C*H*$_3$, 8 ^{2}-C*H*$_3$, 17 ^{6}-C*H*$_2$, 17 ^{8}-C*H*$_2$, 18$_1$^{1}-C*H*$_3$, 8$_1$^{2}-C*H*$_3$, 17$_1$^{6}-C*H*$_2$, 17$_1$^{8}-C*H*$_2$); 1.36-1.20 (m, 4H, 17 ^{7}-C*H*$_2$, 17$_1$^{7}-C*H*$_2$). MALDI-TOF, *m/z*: $(M+Na)^+$ 1538.92, calculated for $C_{86}H_{106}N_{11}NaO_{12}P$ 1538.77.

III. ^{1}H NMR Spectra

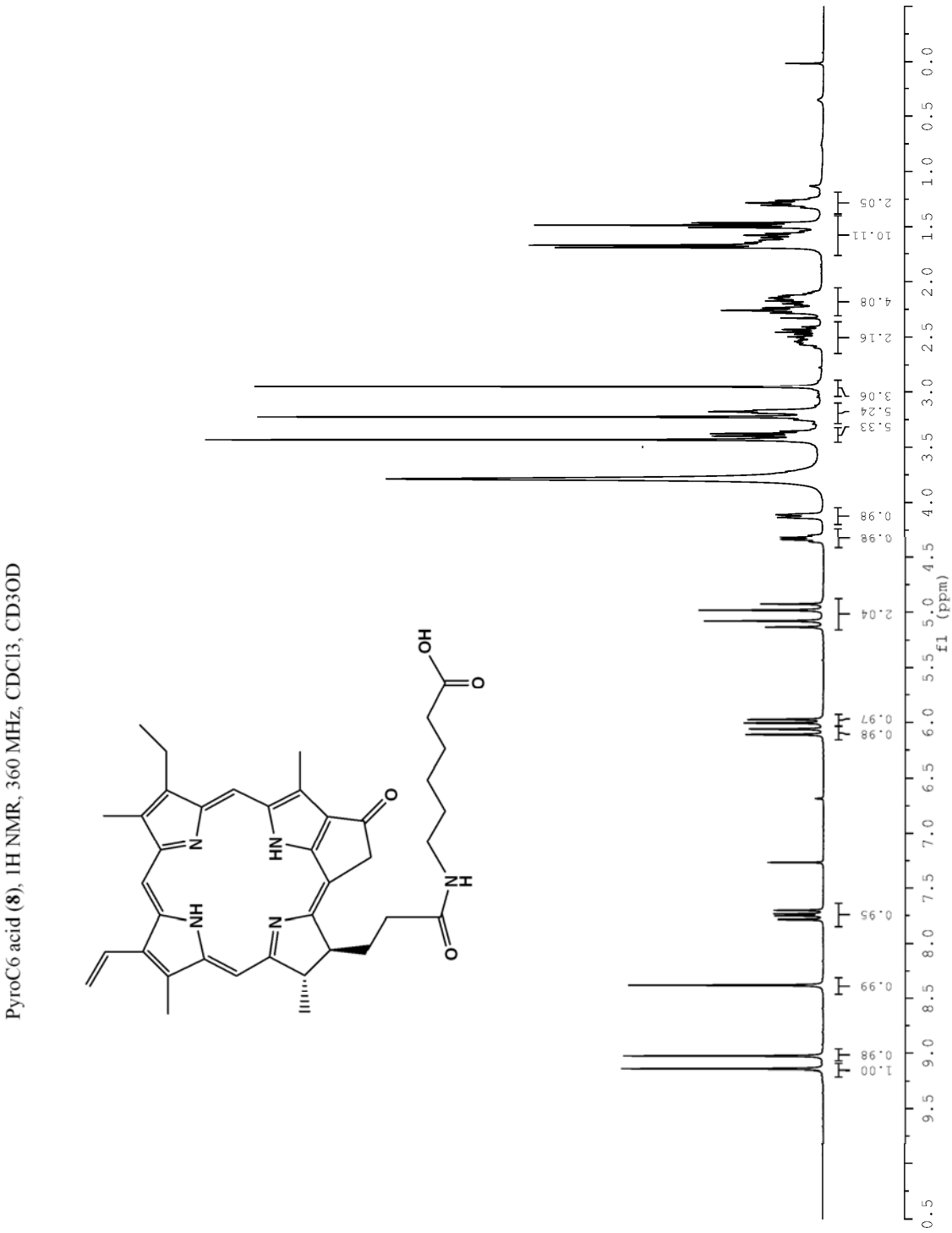

PyroC12 acid (**5**), 1H NMR, 360 MHz, CDCl3, CD3OD

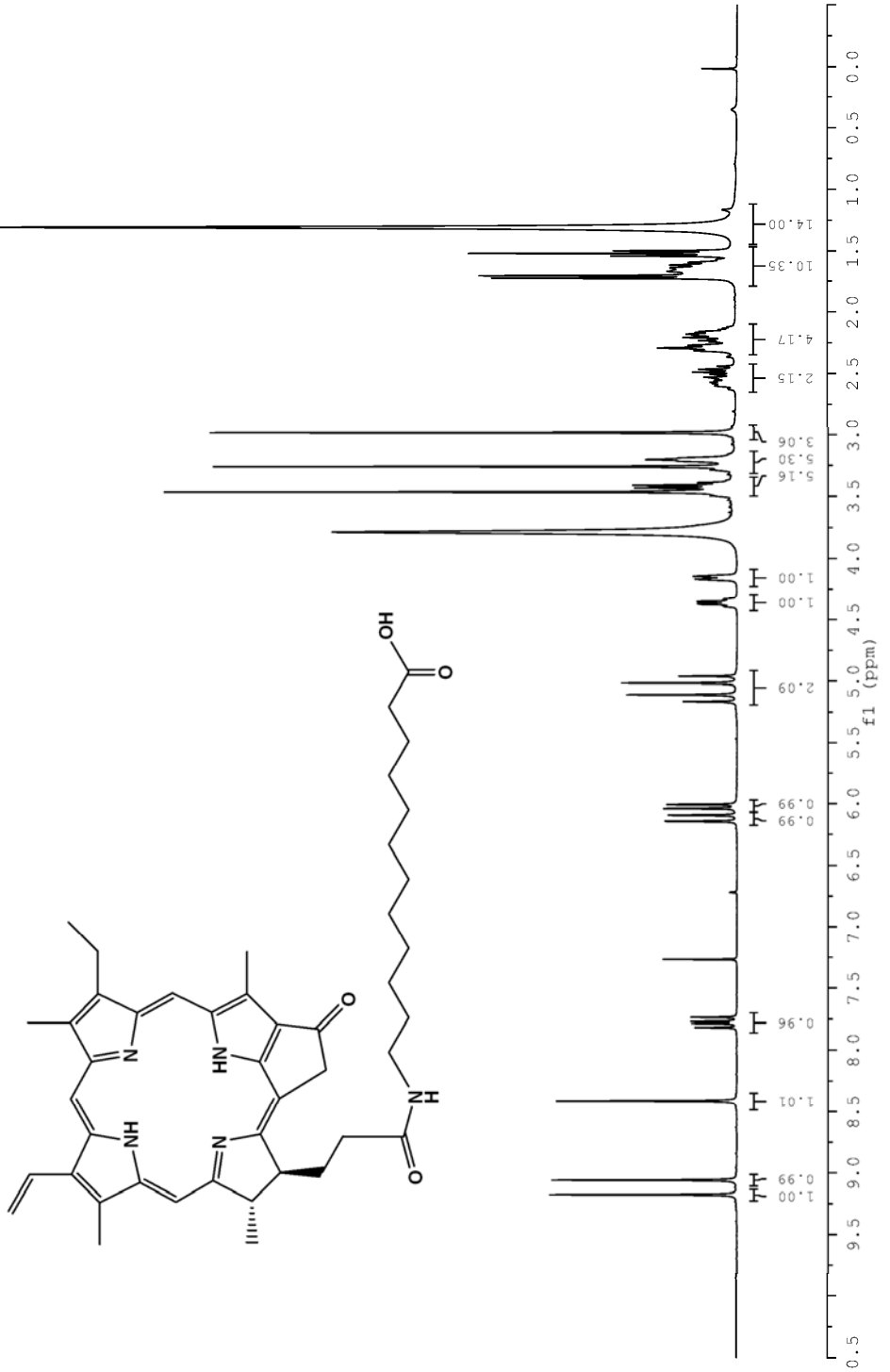

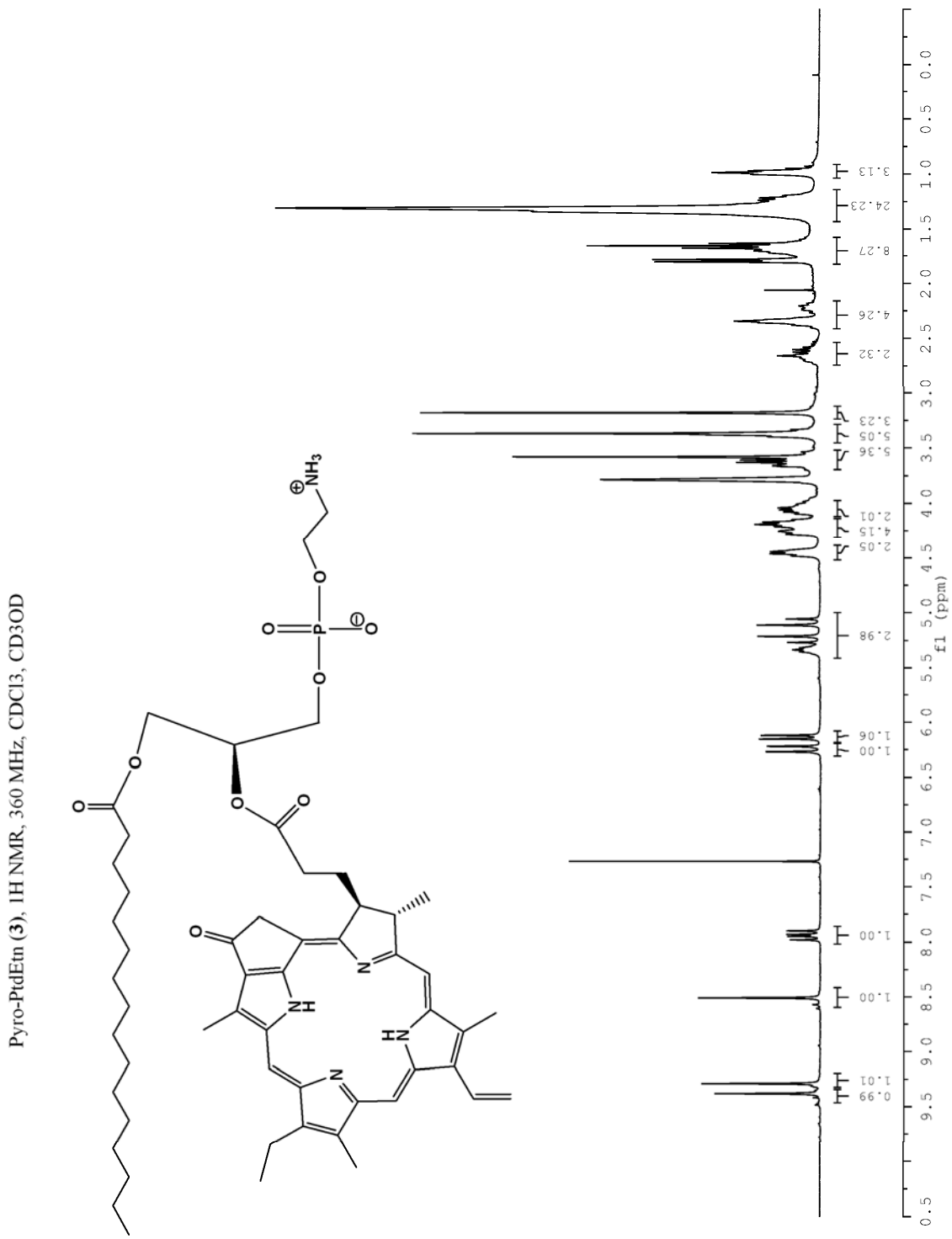
Pyro-PtdEtn (3), 1H NMR, 360 MHz, CDCl3, CD3OD
f1 (ppm)

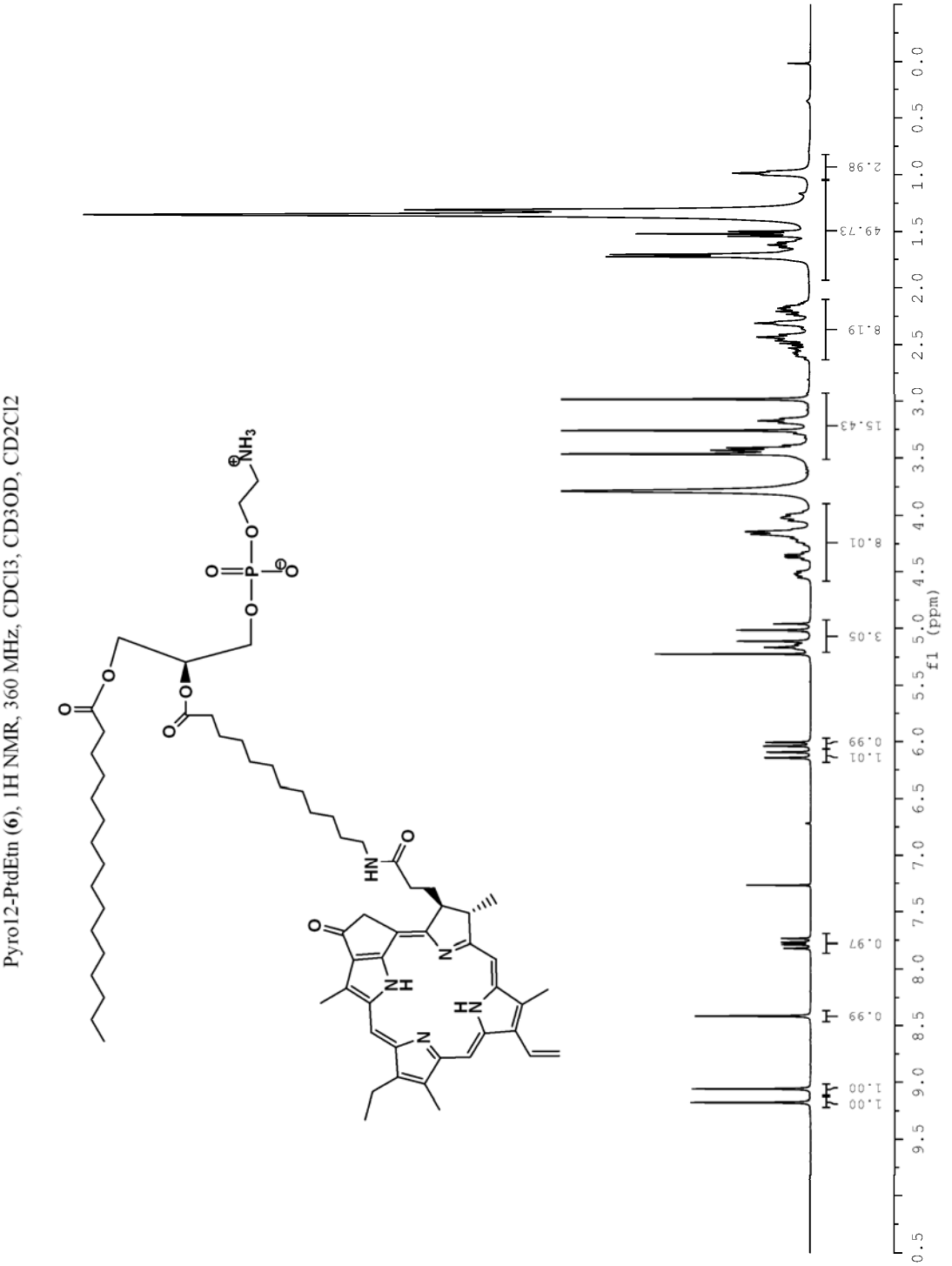
Pyro12-PtdEtn (6), 1H NMR, 360 MHz, CDCl3, CD3OD, CD2Cl2
1.00
1.00
0.99
0.97
1.01
0.99
3.05
8.01
15.43
8.19
49.73
2.98
f1 (ppm)

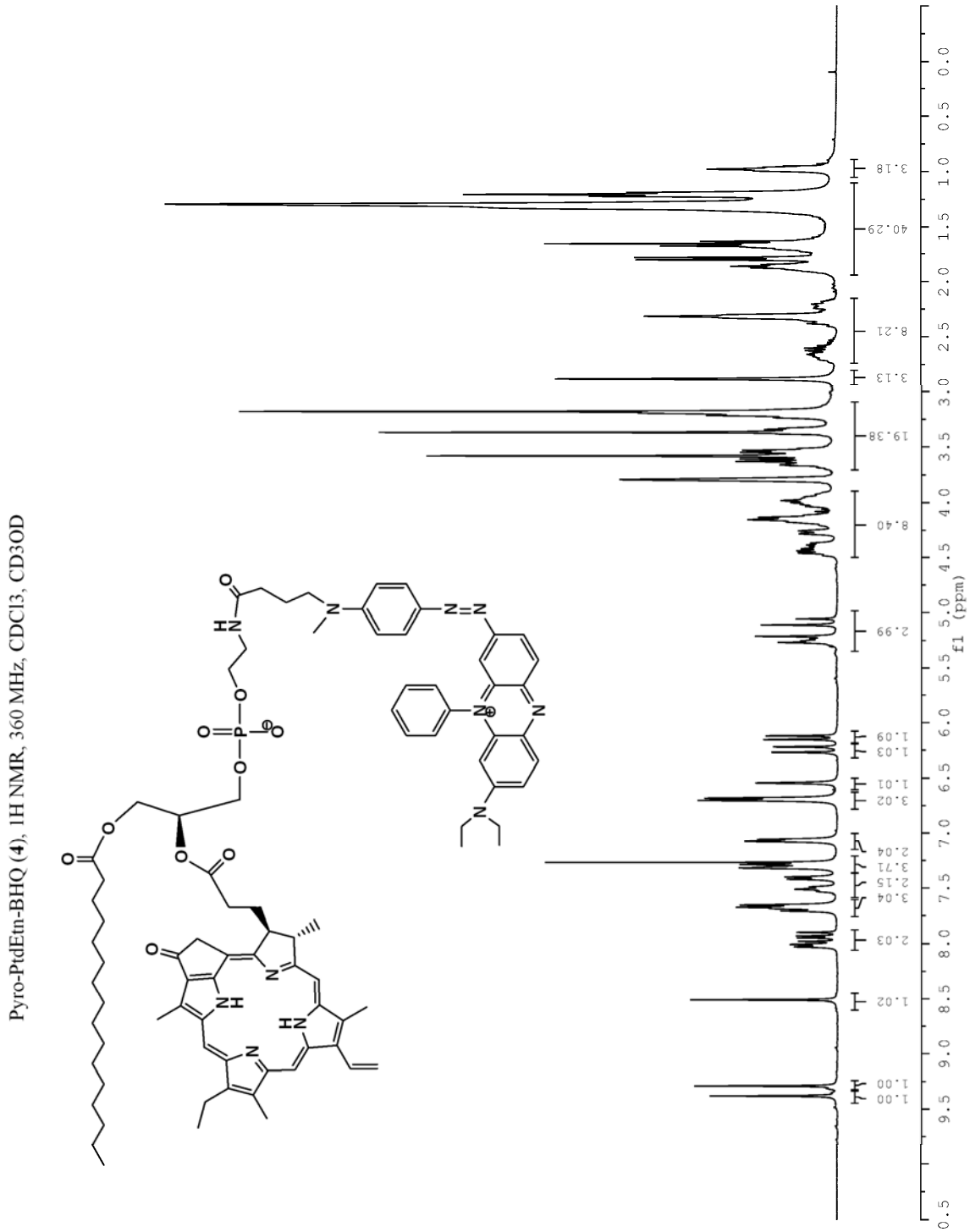
Pyro-PtdEtn-BHQ (4), 1H NMR, 360 MHz, CDCl3, CD3OD
f1 (ppm)

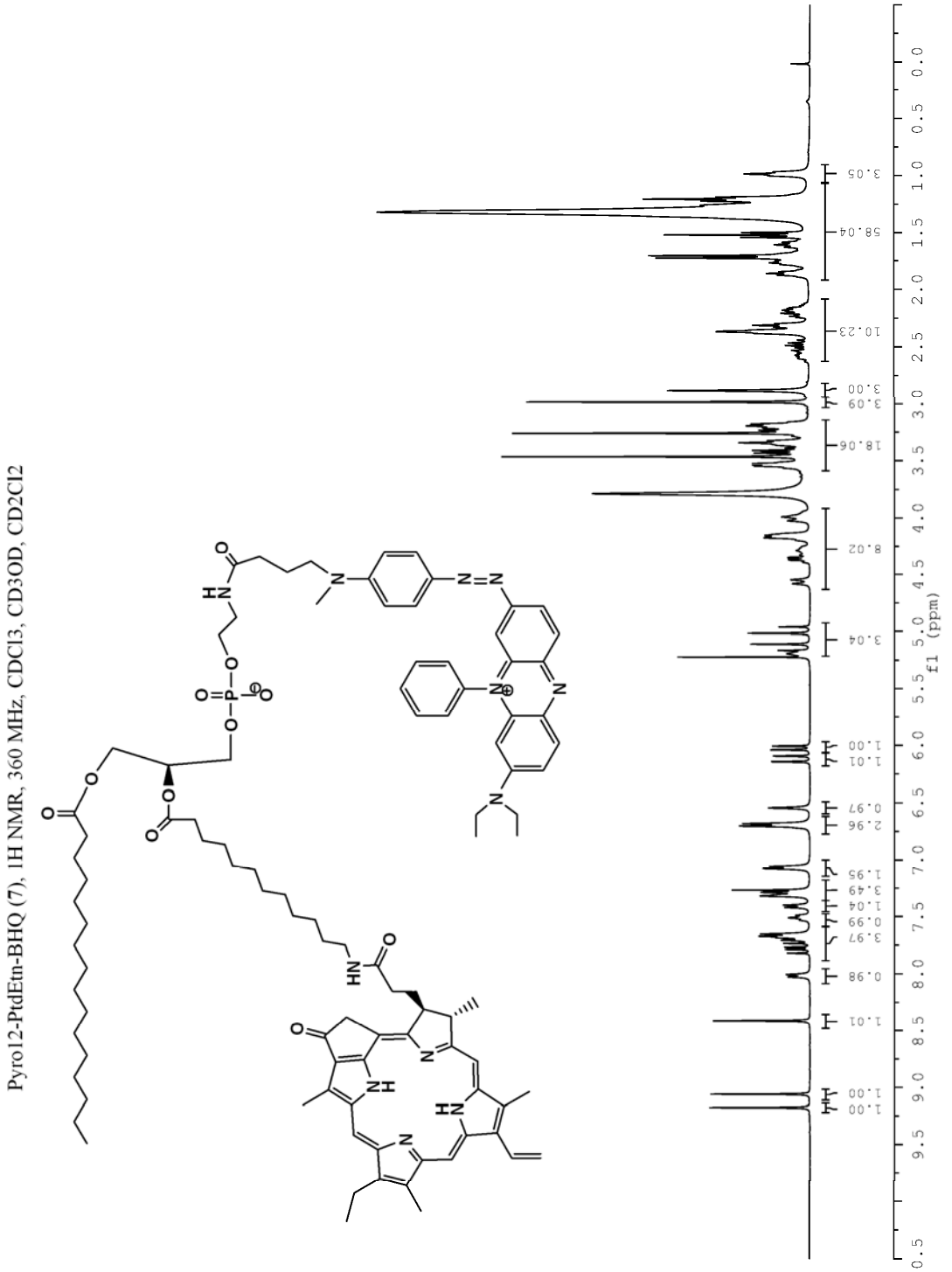
Pyro12-PtdEtn-BHQ (7), 1H NMR, 360 MHz, CDCl3, CD3OD, CD2Cl2
f1 (ppm)

PyroC6-PyroC6-PtdCho (**10**), 1H NMR, 360 MHz, CDCl3, CD3OD, CD2Cl2

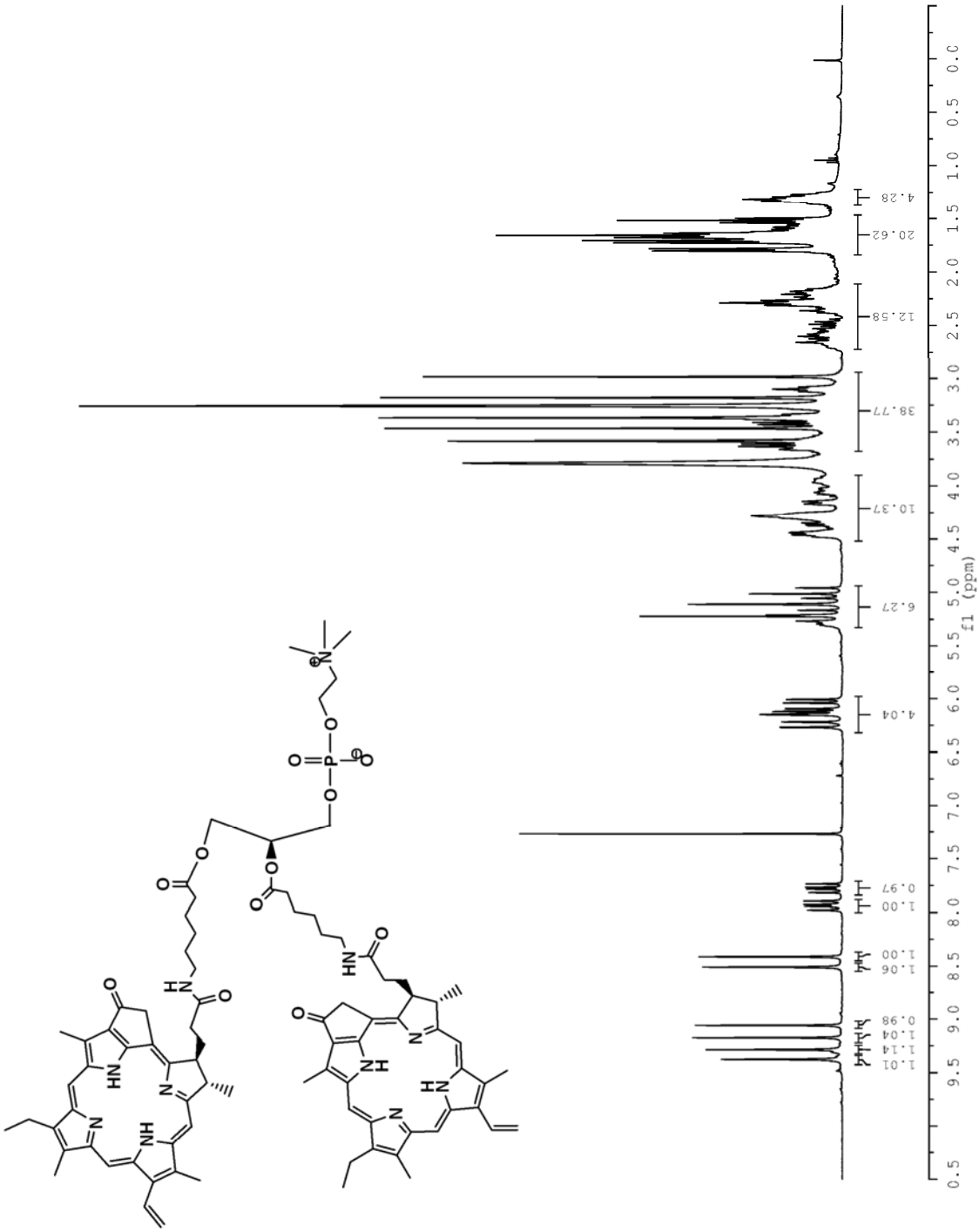

IV. Enzyme mediated probe cleavage

The specificity of each probe to a series of phospholipases was determined by measuring fluorescence release in an *in vitro* assay. Probes were prepared in egg-phosphatidylcholine vesicle by adding fluorophores to a measured amount of egg-PtdCho in chloroform. Probe concentration was determined using the Beer-Lambert law by measuring optical density at 418 nm and using an extinction coefficient of 110,000 $M^{-1}cm^{-1}$. Chloroform was removed by evaporation, and the resulting film was resuspended in 50 mM Tris-HCl, pH 7.4, sonicated and vortexed until optically clear. The final concentration was 1 μM self-quenched phospholipid probe in 50 μM egg-yolk-PtdCho vesicles (i.e. mole fraction of 0.02). Lipid dispersions were aliquotted into 96-well plates at volumes of 100 μL. Reaction mixtures were incubated for 10 minutes at 37°C and reactions were started by addition of 10U of enzyme. The time-dependent release of fluorescence was measured using a Molecular Devices SpectraMax M5 fluorescent plate reader (λ_{Ex} 418 nm, λ_{Em} 675 nm for the Pyro-derivatives, λ_{Ex} 488 nm, λ_{Em} 530 nm for the BODIPY- derivatives).

V. References

(1) Zheng, G.; Li, H.; Zhang, M.; Lund-Katz, S.; Chance, B.; Glickson, J. D. *Bioconjugate Chem.* **2002**, *13*, 392-396.

RESET

REPORT OF INVENTIONS AND SUBCONTRACTS

(Pursuant to "Patent Rights" Contract Clause) (See Instructions on back)

Form Approved
OMB No. 9000-0095
Expires Aug 31, 2001

PLEASE DO NOT RETURN YOUR COMPLETED FORM TO THIS ADDRESS. RETURN COMPLETED FORM TO THE CONTRACTING OFFICER.

1.a. NAME OF CONTRACTOR/SUBCONTRACTOR	c. CONTRACT NUMBER	2.a. NAME OF GOVERNMENT PRIME CONTRACTOR	c. CONTRACT NUMBER	3. TYPE OF REPORT *(X one)*
				☐ a. INTERIM ☐ b. FINAL

b. ADDRESS *(Include ZIP Code)*	d. AWARD DATE *(YYYYMMDD)*	b. ADDRESS *(Include ZIP Code)*	d. AWARD DATE *(YYYYMMDD)*	4. REPORTING PERIOD *(YYYYMMDD)*
				a. FROM
				b. TO

SECTION I - SUBJECT INVENTIONS

5. "SUBJECT INVENTIONS" REQUIRED TO BE REPORTED BY CONTRACTOR/SUBCONTRACTOR *(If "None," so state)*

NAME(S) OF INVENTOR(S) *(Last, First, Middle Initial)* a.	TITLE OF INVENTION(S) b.	DISCLOSURE NUMBER, PATENT APPLICATION SERIAL NUMBER OR PATENT NUMBER c.	ELECTION TO FILE PATENT APPLICATIONS *(X)* d.				CONFIRMATORY INSTRUMENT OR ASSIGNMENT FORWARDED TO CONTRACTING OFFICER *(X)* e.	
			(1) UNITED STATES		(2) FOREIGN			
			(a) YES	(b) NO	(a) YES	(b) NO	(a) YES	(b) NO
			☐	☐	☐	☐	☐	☐
			☐	☐	☐	☐	☐	☐
			☐	☐	☐	☐	☐	☐
			☐	☐	☐	☐	☐	☐

f. EMPLOYER OF INVENTOR(S) NOT EMPLOYED BY CONTRACTOR/SUBCONTRACTOR		g. ELECTED FOREIGN COUNTRIES IN WHICH A PATENT APPLICATION WILL BE FILED	
(1) (a) NAME OF INVENTOR *(Last, First, Middle Initial)*	(2) (a) NAME OF INVENTOR *(Last, First, Middle Initial)*	(1) TITLE OF INVENTION	(2) FOREIGN COUNTRIES OF PATENT APPLICATION
(b) NAME OF EMPLOYER	(b) NAME OF EMPLOYER		
(c) ADDRESS OF EMPLOYER *(Include ZIP Code)*	(c) ADDRESS OF EMPLOYER *(Include ZIP Code)*		

SECTION II - SUBCONTRACTS *(Containing a "Patent Rights" clause)*

6. SUBCONTRACTS AWARDED BY CONTRACTOR/SUBCONTRACTOR *(If "None," so state)*

NAME OF SUBCONTRACTOR(S) a.	ADDRESS *(Include ZIP Code)* b.	SUBCONTRACT NUMBER(S) c.	FAR "PATENT RIGHTS" d.		DESCRIPTION OF WORK TO BE PERFORMED UNDER SUBCONTRACT(S) e.	SUBCONTRACT DATES *(YYYYMMDD)* f.	
			(1) CLAUSE NUMBER	(2) DATE *(YYYYMM)*		(1) AWARD	(2) ESTIMATED COMPLETION

SECTION III - CERTIFICATION

7. CERTIFICATION OF REPORT BY CONTRACTOR/SUBCONTRACTOR *(Not required if: (X as appropriate)* ☐ **SMALL BUSINESS** ☐ **NON-PROFIT ORGANIZATION**

I certify that the reporting party has procedures for prompt identification and timely disclosure of "Subject Inventions," that such procedures have been followed and that all "Subject Inventions" have been reported.

a. NAME OF AUTHORIZED CONTRACTOR/SUBCONTRACTOR OFFICIAL *(Last, First, Middle Initial)*	b. TITLE	c. SIGNATURE	d. DATE SIGNED

DD FORM 882 INSTRUCTIONS

GENERAL

This form is for use in submitting INTERIM and FINAL invention reports to the Contracting Officer and for use in reporting the award of subcontracts containing a "Patent Rights" clause. If the form does not afford sufficient space, multiple forms may be used or plain sheets of paper with proper identification of information by item number may be attached.

An INTERIM report is due at least every 12 months from the date of contract award and shall include (a) a listing of "Subject Inventions" during the reporting period, (b) a certification of compliance with required invention identification and disclosure procedures together with a certification of reporting of all "Subject Inventions," and (c) any required information not previously reported on subcontracts containing a "Patent Rights" clause.

A FINAL report is due within 6 months if contractor is a small business firm or domestic nonprofit organization and within 3 months for all others after completion of the contract work and shall include (a) a listing of all "Subject Inventions" required by the contract to be reported, and (b) any required information not previously reported on subcontracts awarded during the course of or under the contract and containing a "Patent Rights" clause.

While the form may be used for simultaneously reporting inventions and subcontracts, it may also be used for reporting, promptly after award, subcontracts containing a "Patent Rights" clause.

Dates shall be entered where indicated in certain items on this form and shall be entered in six or eight digit numbers in the order of year and month (YYYYMM) or year, month and day (YYYYMMDD). Example: April 1999 should be entered as 199904 and April 15, 1999 should be entered as 19990415.

1.a. Self-explanatory.

1.b. Self-explanatory.

1.c. If "same" as Item 2.c., so state.

1.d. Self-explanatory.

2.a. If "same" as Item 1.a., so state.

2.b. Self-explanatory.

2.c. Procurement Instrument Identification (PII) number of contract (DFARS 204.7003).

2.d. through 5.e. Self-explanatory.

5.f. The name and address of the employer of each inventor not employed by the contractor or subcontractor is needed because the Government's rights in a reported invention may not be determined solely by the terms of the "Patent Rights" clause in the contract.

Example 1: If an invention is made by a Government employee assigned to work with a contractor, the Government rights in such an invention will be determined under Executive Order 10096.

Example 2: If an invention is made under a contract by joint inventors and one of the inventors is a Government employee, the Government's rights in such an inventor's interest in the invention will also be determined under Executive Order 10096, except where the contractor is a small business or nonprofit organization, in which case the provisions of 35 U.S.C. 202(e) will apply.

5.g.(1) Self-explanatory.

5.g.(2) Self-explanatory with the exception that the contractor or subcontractor shall indicate, if known at the time of this report, whether applications will be filed under either the Patent Cooperation Treaty (PCT) or the European Patent Convention (EPC). If such is known, the letters PCT or EPC shall be entered after each listed country.

6.a. Self-explanatory.

6.b. Self-explanatory.

6.c. Self-explanatory.

6.d. Patent Rights Clauses are located in FAR 52.227.

6.e. Self-explanatory.

6.f. Self-explanatory.

7. Certification not required by small business firms and domestic nonprofit organizations.

7.a. through 7.d. Self-explanatory.